Statistical properties of the surface velocity field in the northern Gulf of Mexico sampled by GLAD drifters

Mariano, A.J.; Ryan, E.H.; Huntley, H.S.; Laurindo, L.C.; Coelho, E.; Ozgokmen, TM; Berta, M.; Bogucki, D; Chen, S.S.; Curcic, M.

DOI
10.1002/2015JC011569

Publication date
2016

Document Version
Final published version

Published in
Journal Of Geophysical Research-Oceans

Citation (APA)
Mariano, A. J., Ryan, E. H., Huntley, H. S., Laurindo, L. C., Coelho, E., Ozgokmen, TM., Berta, M., Bogucki, D., Chen, S. S., Curcic, M., Drouin, K. L., Gough, M., Haus, BK., Haza, A. C., Hogan, P., Iskandarani, M., Jacobs, G., Kirwan Jr., A. D., Laxague, N., ... Wei, M. (2016). Statistical properties of the surface velocity field in the northern Gulf of Mexico sampled by GLAD drifters. *Journal Of Geophysical Research-Oceans*, *121*(7), 5193-5216. https://doi.org/10.1002/2015JC011569

AGU PUBLICATIONS

JGR

Journal of Geophysical Research: Oceans

RESEARCH ARTICLE

10.1002/2015JC011569

Special Section:
Physical Processes Responsible for Material Transport in the Gulf of Mexico for Oil Spill Applications

Statistical properties of the surface velocity field in the northern Gulf of Mexico sampled by GLAD drifters

A. J. Mariano[1], E. H. Ryan[1], H. S. Huntley[2], L.C. Laurindo[1], E. Coelho[3,4], A. Griffa[5], T. M. Özgökmen[1], M. Berta[5], D. Bogucki[6], S. S. Chen[1], M. Curcic[1], K.L. Drouin[1], M. Gough[1], B. K. Haus[1], A. C. Haza[1], P. Hogan[4], M. Iskandarani[1], G. Jacobs[4], A. D. Kirwan Jr.[2], N. Laxague[1], B. Lipphardt Jr.[2], M. G. Magaldi[5,7], G. Novelli[1], A. Reniers[8], J. M. Restrepo[9], C. Smith[1], A. Valle-Levinson[10], and M. Wei[4]

[1]Rosenstiel School of Marine & Atmospheric Science, University of Miami, Miami, Florida, USA, [2]College of Earth, Ocean, and Environment, University of Delaware, Newark, Delaware, USA, [3]CMRE-STO, NATO, La Spezia, Italy, [4]Naval Research Labortory, Stennis Space Center, Hancock, Mississippi, USA, [5]CNR-ISMAR, La Spezia, Italy, [6]Department of Physical and Environmental Sciences, Texas A&M University, Corpus Christi, Texas, USA, [7]Department of Earth and Planetary Sciences, Johns Hopkins University, Baltimore, Maryland, USA, [8]Environmental Fluid Mechanics, Delft University of Technology, Delft, Netherlands, [9]Department of Mathematics, Oregon State University, Corvallis, Oregon, USA, [10]Civil and Coastal Engineering Department, University of Florida, Gainesville, Florida, USA

Key Points:
- Velocity statistics are heterogenous, nonstationary, non-Gaussian, and a strong function of feature sampled, topography, & wind forcing
- Large velocity variance, anisotropic velocity statistics, and horizontal diffusivity values of O(10^5)m^2/s are observed at bifurcations
- Fast transport pathways exist between the northern Gulf of Mexico and the southern Gulf of Mexico

Correspondence to:
A. J. Mariano,
amariano@rsmas.miami.edu

Citation:
Mariano, A. J., et al. (2016), Statistical properties of the surface velocity field in the northern Gulf of Mexico sampled by GLAD drifters, *J. Geophys. Res. Oceans*, *121*, 5193–5216, doi:10.1002/2015JC011569.

Received 16 DEC 2015
Accepted 13 JUN 2016
Accepted article online 16 JUN 2016
Published online 30 JUL 2016

Abstract The Grand LAgrangian Deployment (GLAD) used multiscale sampling and GPS technology to observe time series of drifter positions with initial drifter separation of O(100 m) to O(10 km), and nominal 5 min sampling, during the summer and fall of 2012 in the northern Gulf of Mexico. Histograms of the velocity field and its statistical parameters are non-Gaussian; most are multimodal. The dominant periods for the surface velocity field are 1–2 days due to inertial oscillations, tides, and the sea breeze; 5–6 days due to wind forcing and submesoscale eddies; 9–10 days and two weeks or longer periods due to wind forcing and mesoscale variability, including the period of eddy rotation. The temporal *e*-folding scales of a fitted drifter velocity autocorrelation function are bimodal with time scales, 0.25–0.50 days and 0.9–1.4 days, and are the same order as the temporal *e*-folding scales of observed winds from nearby moored National Data Buoy Center stations. The Lagrangian integral time scales increase from coastal values of 8 h to offshore values of approximately 2 days with peak values of 3–4 days. The velocity variance is large, $O(1)\ m^2/s^2$, the surface velocity statistics are more anisotropic, and increased dispersion is observed at flow bifurcations. Horizontal diffusivity estimates are $O(10^3)\ m^2/s$ in coastal regions with weaker flow to $O(10^5)\ m^2/s$ in flow bifurcations, a strong jet, and during the passage of Hurricane Isaac. The Gulf of Mexico surface velocity statistics sampled by the GLAD drifters are a strong function of the feature sampled, topography, and wind forcing.

1. Introduction

The surface velocity field offshore of Louisiana, Mississippi, Alabama, and Florida in the northern Gulf of Mexico (GoM) is of great practical and scientific interest for a number of reasons including the offshore oil industry, heavy shipping due to its proximity to the Mississippi River, its influence on weather, especially hurricane development, and coastal regions of hypoxia. The Loop Current, Loop Current rings, and mesoscale eddies are the dominant flow features offshore of the continental shelf [*Sturges and Lugo-Fernandez*, 2005; *Sturges and Kenyon*, 2008]. These large flow features have been extensively documented because they are seen in satellite-based sea temperatures, altimetric, and ocean color measurements. It is evident in these observations that the mesoscale eddies influence the flow on the continental shelf.

A very large experiment consisting of 750 ARGOS-tracked CODE-like drifters drogued at a nominal depth of 0.5 *m*, was conducted over a 6 year period from 1993 to 1998. The drifters were deployed in different regions of the northern GoM: Louisiana-Texas shelf; the Mississippi delta region; and Florida's Big Bend region of the northern GoM shelf as part of the Surface CUrrent and Lagrangian drift Program (SCULP) [*Ohlmann and Niiler*, 2005] in order to learn about the shelf circulation. Some of the primary results from SCULP are that the flow on the shelf is forced by synoptic scale weather systems, has a seasonal component, and eddies are important for cross-shelf transport. *DiMarco et al.* [2005] analyzed 1397 drifters in the GoM that were mostly drogued at 50 m and found that the flow is highly variable over most of the GoM, and

that there is a strong seasonal signal in the western GoM due to changes in wind stress. These studies suggest that the average surface velocity field in the northern and western GoM is primarily determined by the winds, while the average surface velocity in the eastern GoM is set by the Loop Current system. At the boundaries of these regimes, such as the continental shelf in the northern GoM near the DeSoto canyon, the surface velocity is a function of both wind forcing and the energetic eddy field associated with the Loop Current system [*Carnes et al*., 2008].

Average surface velocity fields, as well as the dispersion quantities estimated from velocity data, are important for search and rescue operations performed by the U.S. Coast Guard, modeling the dispersion of fish larvae from spawning sites of large pelagic fish, and predicting the spread of pollutants. For example, following the tragic Deepwater Horizon oil rig explosion on 20 April 2010, oil gushed from the bottom of the GoM at a depth of 1500 m, latitude 28.74° N and longitude 88.32° W, for 87 days before it was capped. The oil surfaced and was transported and dispersed onshore and offshore from its release location by variable winds, waves, and the energetic flow field. The surface distribution of oil was driven by coastal to ocean dynamics that varied from slow flow to strong energetic eddies. Predictions of oil spreading were used to target the response to minimize the spill's impact, especially near the coast. Large deviations between predicted and observed oil locations indicated that sufficient real-time, high-resolution velocity data, and better model parameterizations of turbulent processes at small scales would both be needed for better oil spreading forecasts [*Mariano et al*., 2011]. These parameters vary both spatially in the northern GoM, and temporally due to the variability in atmospheric forcing, especially during strong atmospheric events, such as the passage of fronts and hurricanes. Reliable estimates of turbulent dispersion parameters for a broadband energetic, highly variable geophysical flow field require a large amount of high-resolution data.

CARTHE, the Consortium for Advanced Research on the Transport of Hydrocarbon in the Environment funded by the Gulf of Mexico Research Initiative, conducted a targeted experiment in July 2012, guided by data-assimilative ocean forecast models [*Jacobs et al*., 2014; *Coelho et al*., 2015], real-time hydrography, and satellite images, and a suite of upper ocean measurements [*Özgökmen et al*., 2014] that included over 300 drifters of various designs. 297 CODE-style drifters [*Davis*, 1985], that are 1m tall and 1m wide composed of orthogonal sails that extend radially in four directions and span the water column between 0.2 and 1.2 m, were deployed around the site of the DWH spill in the DeSoto Canyon in the northern GoM (Figure 1). This Grand LAgrangian Deployment (GLAD) used multiscale sampling and GPS devices manufactured by SPOT technologies to observe a time series of drifter positions at very high spatio-temporal resolution. It was designed to estimate dispersion statistics, resolving both submesoscale and mesoscale motions through deployment stencils sampling horizontal scales from 100 m to 10 km (Figure 1), with a nominal temporal sampling resolution of 5 min. A detailed analysis of the surface velocities and related transport using a blend of drifter and altimetric-based velocity estimates for the GLAD experiment is discussed in *Berta et al*. [2015] and *Olascoaga et al*. [2013] , and the relative dispersion statistics calculated from the GLAD drifters are the primary focus of *Poje et al*. [2014].

The focus of this paper is the spatial variation and distribution of the basic statistics of the horizontal (zonal, meridional) velocity field $\mathbf{V}(x,y,t)=(u(x,y,t),v(x,y,t))$ derived from the positions $\mathbf{X_i}(t)=(x_i(t),y_i(t))$ from drifters $i=1,2\ldots,n=297$. The fundamental velocity statistics calculated for each GLAD drifter and for each velocity component are the mean flow and its temporal variance, Lagrangian velocity autocorrelation function and its *e*-folding scale, dominant period of motion, integral time scale, and horizontal diffusivity. It is assumed that the mean flow changes linearly in time over each data segment and that the second-order statistics are stationary for 1 month. This assumption is most suspect for data segments that include trajectories in the path of Hurricane Isaac. Spatial maps of the estimated statistics for our study region are presented. The frequency distribution of the primary statistical parameters of the surface velocity field are tabulated, yielding insight into the prior probability density functions needed for Bayesian-based analysis and data assimilation methods. The temporal variation of absolute dispersion is also calculated for four sets of drifter clusters. The source and processing of the data are described in section 2, the estimation methodology is described in section 3, the resulting estimates are shown and discussed in section 4, and concluding remarks are given in section 5.

2. Data

The primary Lagrangian component of GLAD consisted of 297 GPS-equipped, CODE-style drifters with a nominal position accuracy of 5 m, transmitting every 5–15 min with near real-time data delivery, and a

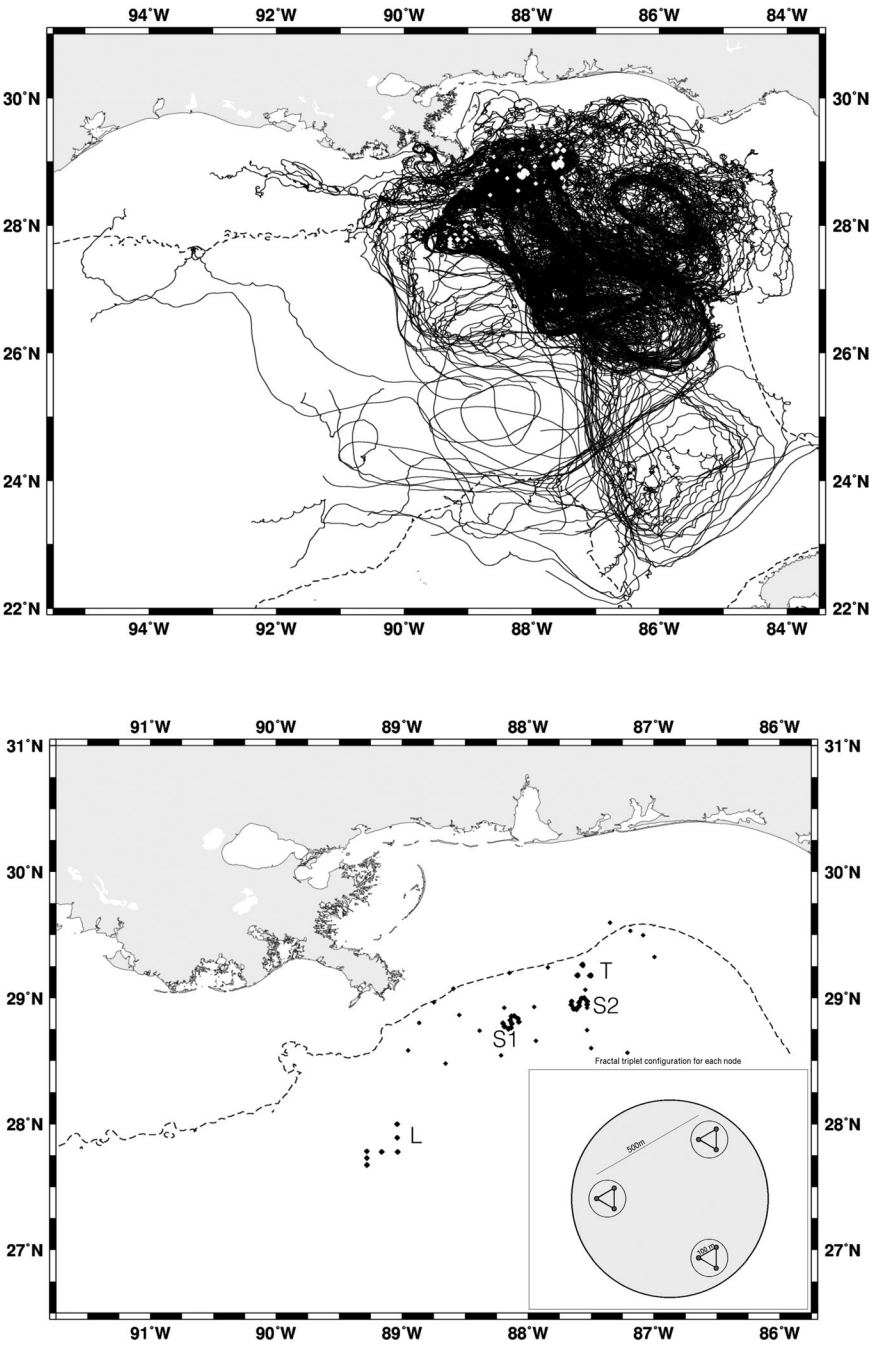

Figure 1. (top) Spaghetti plot of the GLAD drifters used in this analysis. The black lines are the GLAD drifter trajectories that are mostly 2–3 months in length. The 300 m isobath contour is shown as a dashed line, land and the launch locations, primarily offshore of 300 m depth and near 89°W, 28°N, are plotted in shades of grey for the northern GoM. The coastline of Louisiana, Mississippi, Alabama, and the western Florida "panhandle and Big-Bend region" are visible in the north, as well as parts of western Cuba in the southeast corner of the plot. (middle) The details of the survey launches, S1, S2, L, and T deployments with larger diamonds implying nodes. The inset is the deployment pattern of the nodes consisting of 3 sets of triplets spaced 500 m apart with 100 m spacing for the triplets. (bottom) The average position for all of the 31 day data segments used for analysis are plotted.

nominal battery life that exceeded 2 months [*Özgökmen*, 2012]. Other drifters with different designs were also deployed, but they were not included in this analysis. GLAD drifters were deployed from 20 to 31 July 2012 during the same season as the latter portion of the DWH event, which was active from 20 April to 15 July 2010. Two sets of 90 drifters each arranged in an S pattern were released offshore of the shelf break in the region near the DWH site (Figure 1). The S track consisted of 10 nodes spaced at 2 km, with each node

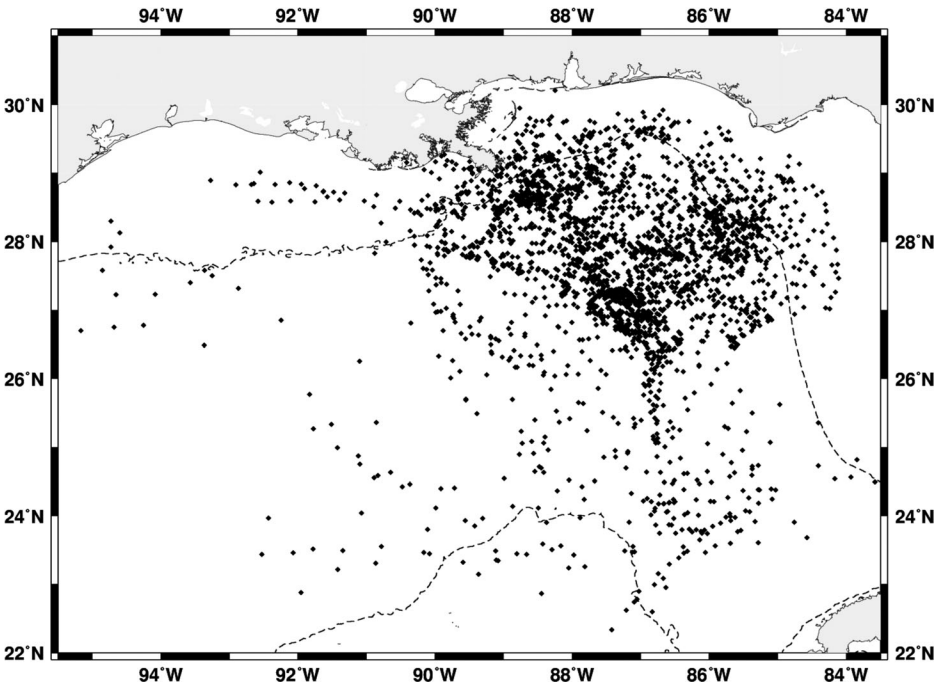

Figure 1. (continued)

containing nine drifters deployed in three 500 m equilateral triangles with drifter triplets launched at a nominal 100 m separation. These drifters were deployed in two regions, S1 and S2, that spanned 8 by 10 km. Other drifter deployments included an initial larger-scale survey and two multiscale, nodal deployments; the T deployment that targeted cross-shelf transport near the northern tip of the DeSoto Canyon with drifter nodes deployed along a triangular-shaped pattern, and the L deployment sampling a strong cyclone in deeper water (Figure 1, middle). The choice of sampling pattern was guided by numerical simulations using data-assimilative models [*Jacobs et al*., 2014; *Özgökmen et al*., 2014]. Drifters were launched from the R/V Walton Smith and two small boats allowing the deployment of 90 drifters in a span of 5 h. This deployment pattern of a large scale survey and different deployments of tight clusters allowed simultaneous sampling at multiple separation scales, initially on the order of 100 m to 10's of km, which then permitted sampling of different dynamical features.

Besides occasional bad data transmission due to weather and shipping traffic, there were a few drifters abducted by boaters in the region and some of these were redeployed yielding some very large observed velocities due to the ten to twenty knot boat speeds. The raw data were edited and the trajectories were filtered using the techniques described by *Yaremchuk and Coelho* [2015] yielding a 3 months long data set with a temporal resolution of 15 min. The estimated velocity error is a few cm/s [*Yaremchuk and Coelho*, 2015]. The filtering preserves the energy for periods of 1 h and greater. The data density starts with 289 drifters from the last week of July 2012 available for our analysis. 130 drifters lasted at least 2 months, surviving the passage of Hurricane Isaac through the area during 27–29 August 2012. The dispersion of the GLAD drifters over the next 3 months provided five million position data points that spanned submesoscale and mesoscale dynamics yielding unprecedented statistics of the surface velocity field, absolute dispersion, and relative dispersion over a broad-band of energetic scales [*Poje et al*., 2014].

A spaghetti plot of the GLAD drifters (Figure 1, top) contains a densely sampled area near and offshore of the 300 m isobath. Visual inspection of trajectories confirms that the drifters sampled inertial motion especially along the shelf break, submesoscale and mesoscale eddies, the background flow, and a southeast/south energetic jet in the region that spans from the coastal zone to the deeper central GoM. About 20 drifters left the primary study region and dispersed widely. A dozen drifters visited water depths shallower than 300 m near the Yucatan Peninsula, suggesting a very efficient pathway from the northern GoM to the Yucatan Shelf created by the mesoscale eddies and the southeast/south jet. Similar pathways connecting

the northern GoM with deeper waters have been found in numerical models [*Toner et al*., 2003], altimetry products [*Berta et al*., 2015], and satellite images of chlorophyll plumes [*Toner et al*., 2003]. Typically, the efficient pathways are created by a combination of strong dynamical features.

2.1. Lagrangian-Based Statistical Analysis

The large geographic region that was sampled along with the range of characteristics of the observed trajectories suggest that the velocity statistics will also have considerable variations. Any estimation method needs to preserve this large variability and not reduce it by Eulerian-based averaging of heterogenous dynamical features [*Mariano and Chin*, 1996]. A Lagrangian-based approach, where all of the estimated quantities were calculated from segments of the position and velocity time series for each drifter, was adopted for this study. The length of the data segments used for estimation is a classic variance-resolution trade-off. *LaCasce and Ohlmann* [2003] used 25 days in their analysis. Here 31 days was selected, balancing the need for enough data in time to reliably estimate the autocorrelation function, and the need for sufficient distinct data segments to provide adequate spatial resolution for the maps shown below. The arithmetic average of the longitude and latitude positions for all of the 31 day segments are plotted in the Figure 1 (bottom). LaCasce and Ohlmann's choice of 25 days was selected for drifters that were, on the average, closer to shore with shorter time scales than the GLAD drifters. Correlation functions estimated using 15-, 20-, and 25 day segments were noisy, and the resulting estimates of correlation parameters contained a number of obvious outliers. Correlation functions estimated from 31 day segments were less noisy and contained fewer outliers. Each drifter trajectory was segmented into a set of six overlapping 31 day time windows, given as 2012 year day/date: (204/22 July, 234/21 August); (219/6 August, 249/5 September); (234/21 August, 264/20 September); (249/5 September, 279/5 October); (264/20 September, 294/20 October); and (279/5 October, 309/4 November).

The average values (Figure 2, bottom), standard deviations, and autocorrelation functions of the u and v velocity components were estimated from each 31 day data segment and for each drifter. The dominant period, temporal e-folding scale, integral time scale, velocity variance, and the total horizontal eddy diffusivity were calculated as described in the next section. The resulting estimates were placed at the arithmetic average calculated from all of the longitude and latitude positions for that time segment in order to produce spatial maps of the dominant statistical parameters of the surface velocity field. Bicubic splines were used to spatially interpolate the irregular distributed estimates.

The drifter trajectories were also segmented into a set of overlapping 10 day time windows (overlap is 5 days) in order to produce another set of mean velocity estimates that better resolve the mesoscale flow features (Figure 2, top). Spatial maps of the average velocities estimated during the GLAD experiment exhibit distinct flow regimes. There was a slow mean flow in the coastal regions, an energetic jet with mostly southward transport centered along 87°W and south of 27° N, the Loop Current just north of Cuba, and strong westward flow offshore of the shelf break west of 91° W due to a Loop Current Eddy (Figures 2 and 3, top). Average surface velocities ranged from 0.2 m/s on the shelf to $O(1\,\mathrm{m/s})$ in the deeper waters. This is consistent with a summertime (July, August, and September) climatological, Eulerian average of archived near-surface drifters data from the Global Drifter Database [*Lumpkin and Pazos*, 2007] (Figure 3, bottom) from the years 1996–2013.

Stronger flow features are more evident in the estimates produced by a new data blending technique (Figure 3, top) that reduces the smoothing inherent in averaging methods (Figure 2). This technique uses 1-D functions to account for cross-stream variations of the mean flow structure within each bin, whose advantage relative to 2-D methods [e.g., *Bauer et al*., 1998; *Lumpkin and Johnson*, 2013] lies in the fact that the fitting operation requires the determination of a smaller number of parameters. Specifically, for the GLAD observations, subsets of the velocity measurements were first selected within circular spatial bins with 0.5° radius centered on the grid points of a regular 0.25° × 0.25° Eulerian grid. The local Cartesian coordinate system was rotated in small angle increments about the data centroid. At each angle, fifth-degree 1-D polynomials were separately fitted to the velocity component aligned with the rotated x-axis. The respective fitting errors were calculated. Estimates of the mean u and v velocity structure were retrieved at the angle where the fitting error is a minimum. For mapping purposes, the 1-D velocity estimates obtained from all bins were interpolated using bicubic splines to a 0.125° × 0.125° grid.

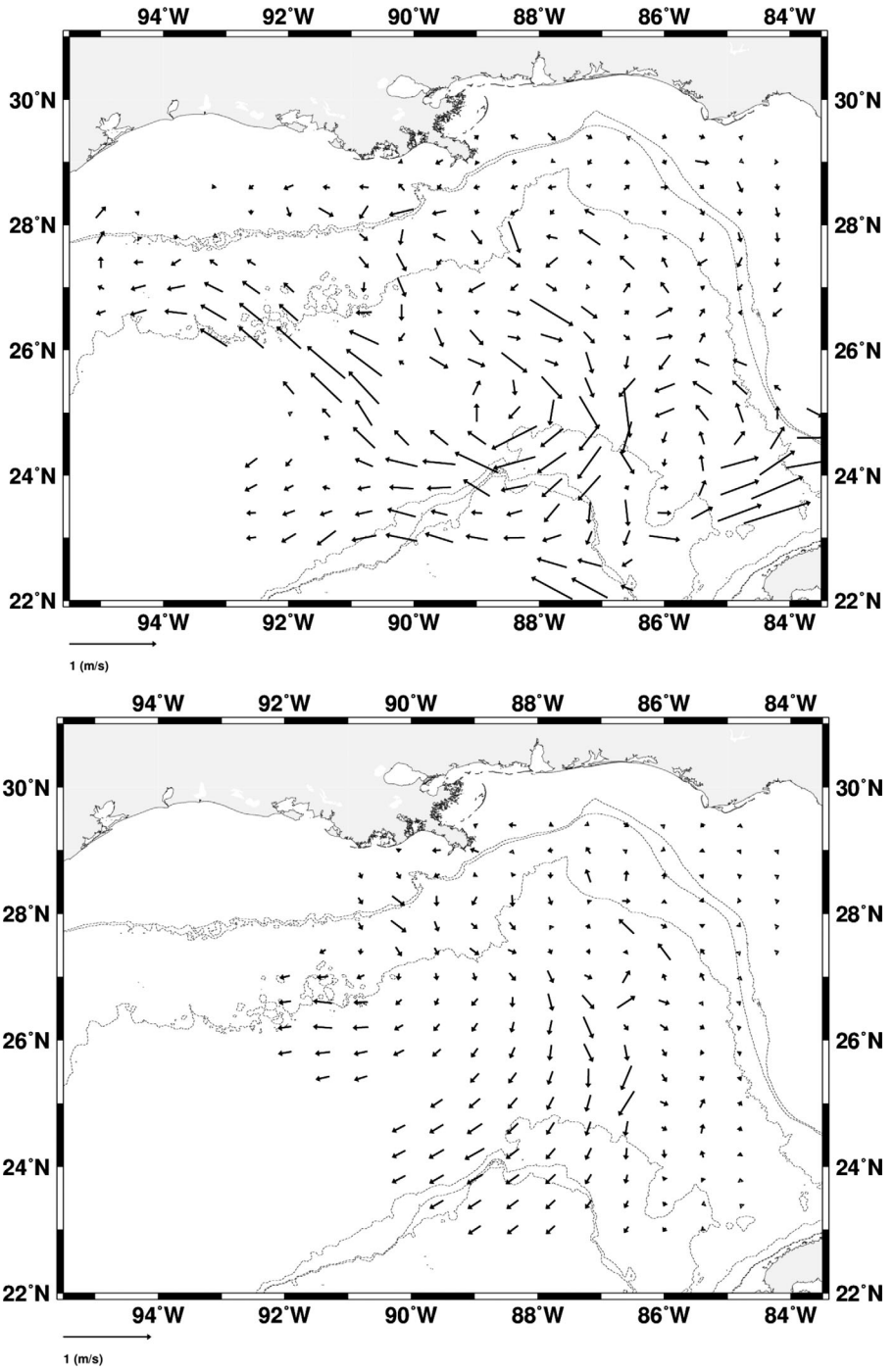

Figure 2. Lagrangian estimate of the average surface velocity during the GLAD experiment in the northern Gulf of Mexico using (top) 10 day data segments and (bottom) 31 day data segments. The 200 m, 300 m, and 2000 m isobath contours are also plotted.

As expected the details of the average velocity maps differ between the different averaging methods. Nevertheless, in all of the maps a strong southward flow, eddies, and flow bifurcation are present. The strong southward flow observed during GLAD extends over a much larger area than climatology. Also, between approximately 88° W to 85° W, 26° N to 28° N there is a cyclonic circulation in the GLAD estimates that is more energetic than the cyclonic circulation in the climatology. The Loop Current was not in its climatological position during the GLAD experiment (or during the 2010 DWH oil spill). Evident in all of these mean velocity maps are regions of flow bifurcations. Flow bifurcations are defined here simply as regions where an organized flow splits into two branches.

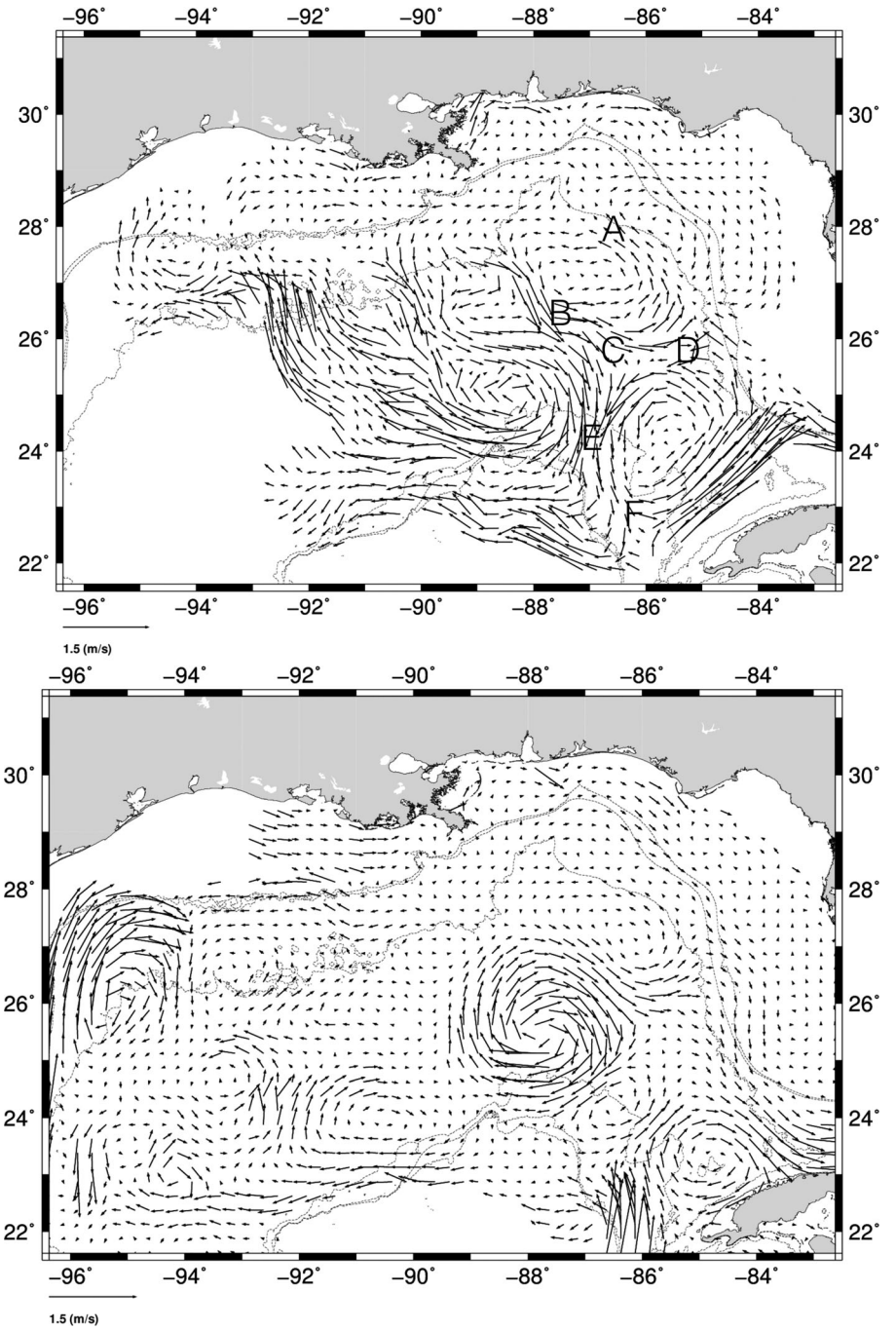

Figure 3. (top) Average velocity from the same GLAD drifter data used in Figure 2, but based on a new localized, minimum-variance, adaptive coordinate system blending technique (see text). The symbols A, B, C, D, E, and F indicate regions of flow bifurcations. (bottom) Climatological average velocity from the Atlantic Oceanographic and Meteorological Laboratory (AOML) archived near-surface drifters for the summer months July, August, and September, and for the years 1996–2013. The 200 m, 300 m, and 2000 m isobath contours are also plotted.

3. Estimation Methodology

Different methods have been used for the estimation of integral time scales and diffusivity from ocean drifters and floats because of the bias-variance tradeoff inherent in using sparse, noisy, and aliased data from a heterogeneous and nonstationary turbulent velocity field [*Davis*, 1987; *Davis*, 1991; *Zhurbas and Oh*, 2003; *Sallée et al.*, 2008; *De Dominicis et al.*, 2012; *Klocher et al.*, 2012; *Chiswell*, 2013]. The approach adopted here is Lagrangian in nature and parsimonious in the sense that the Lagrangian

velocity autocorrelation function is computed by assuming a simple correlation function for each velocity component u and v with just two important parameters; a zero-crossing scale to represent the dominant wave motion and an e-folding scale to parameterize the turbulent component of the flow [*Mariano and Chin*, 1996]. The major disadvantage of our approach is that it is not optimized to remove the effects of horizontal velocity shear that significantly contributes to any measure of particle separation.

An autocorrelation function of the following form is assumed,

$$C(\tau)=a_1\cos\left(\frac{2\pi\tau}{a_2}\right)e^{-\left(\frac{\tau}{a_3}\right)^2}, \tag{1}$$

where τ is the temporal lag. The correlation parameters are $a_1=1-\epsilon$, where $\epsilon=\frac{\sigma_n^2}{\sigma_u^2}$ is the error due to sensor and subgrid scale variability σ_n^2 that results from finite spatio-temporal sampling normalized by the velocity variance σ_u^2; a_2 is the dominant period associated with wavelike and other periodic motion; and a_3 is the temporal e-folding scale associated with turbulent motion. This correlation model does not capture the diurnal variability, due to inertial and tidal motion, seen in the estimated correlation functions (Figure 4). This is not a serious error since the integral of the velocity autocorrelation function for simple oscillatory motion is zero. A more detailed look at the estimation of integral time scales and diffusivity is planned for the future incorporating other data sets and estimation methods.

A feature-based approach [*Mariano and Chin*, 1996] to parameter estimation is used to calculate the dominant period seen in the autocorrelation function and the temporal e-folding scale. The autocorrelation function with the estimated parameters is integrated to calculate the integral time scales. The following description is for the u velocity component, but the method applied to the v velocity is identical. Since the number of data values is finite, equation (1) is discretized. $C(\tau)$ is estimated by $\hat{C}(\tau_k)$ at the k^{th} temporal lag bin, $\tau_k=15k$ min, $k=0,1,\ldots,2880$ for each data segment from each drifter. The correlation function is symmetric, $C(\tau_i)=C(-\tau_i)$, thus only zero and positive discrete lags are considered. A total of 2881 temporal lags are calculated ranging from 0 to 30 days. Data pairs, from all times i and j in each data segment, u_i and u_j are sorted into temporal lag bins τ_k, then $\langle(u_i-\langle u_i\rangle)(u_j-\langle u_j\rangle)\rangle$, $\langle(u_i-\langle u_i\rangle)^2\rangle$, and $\langle(u_j-\langle u_j\rangle)^2\rangle$ are calculated for each temporal lag $k=15|i-j|$ min. The standard arithmetic average is used for calculating the expected value of the covariances and variances.

The discrete autocorrelation and cross-correlation estimates are

$$\hat{C}_{uu}(\tau_k)=\frac{\langle(u_i-\langle u_i\rangle)(u_j-\langle u_j\rangle)\rangle}{(\langle(u_i-\langle u_i\rangle)^2\rangle\langle(u_j-\langle u_j\rangle)^2\rangle)^{1/2}}, \tag{2a}$$

$$\hat{C}_{vv}(\tau_k)=\frac{\langle(v_i-\langle v_i\rangle)(v_j-\langle v_j\rangle)\rangle}{(\langle(v_i-\langle v_i\rangle)^2\rangle\langle(v_j-\langle v_j\rangle)^2\rangle)^{1/2}}, \tag{2b}$$

$$\hat{C}_{uv}(\tau_k)=\frac{\langle(u_i-\langle u_i\rangle)(v_j-\langle v_j\rangle)\rangle}{(\langle(u_i-\langle u_i\rangle)^2\rangle\langle(v_j-\langle v_j\rangle)^2\rangle)^{1/2}}. \tag{2c}$$

$$\hat{C}_{vu}(\tau_k)=\frac{\langle(v_i-\langle v_i\rangle)(u_j-\langle u_j\rangle)\rangle}{(\langle(v_i-\langle v_i\rangle)^2\rangle\langle(u_j-\langle u_j\rangle)^2\rangle)^{1/2}}. \tag{2d}$$

The choice of what mean velocity $(\langle u_i\rangle,\langle v_i\rangle)$ to use in the calculation of the correlation function needs to be made. Choices include (1) using climatological averages for the region, (2) calculating a constant average for each segment of drifter data, (3) fitting a linear temporal trend to the data segments, or (4) using a spatially dependent mean velocity field (e.g., Figures 2 and 3). The question of stationarity of the velocity field and the effects of smearing an Eulerian-based average [*Mariano and Chin*, 1996] rule out choice (1). Most importantly, the climatological near-surface velocity field for the summer months of July, August, and September (Figure 3) does not resemble the flow field during GLAD enough (Figure 2 or 3). The desire to keep the entire estimation procedure in the Lagrangian framework and the principal of parsimony rule out choice (4). The principal of parsimony argues for either a one parameter model for the mean, such as the simple arithmetic average, or a two parameter model such as a linear trend in time.

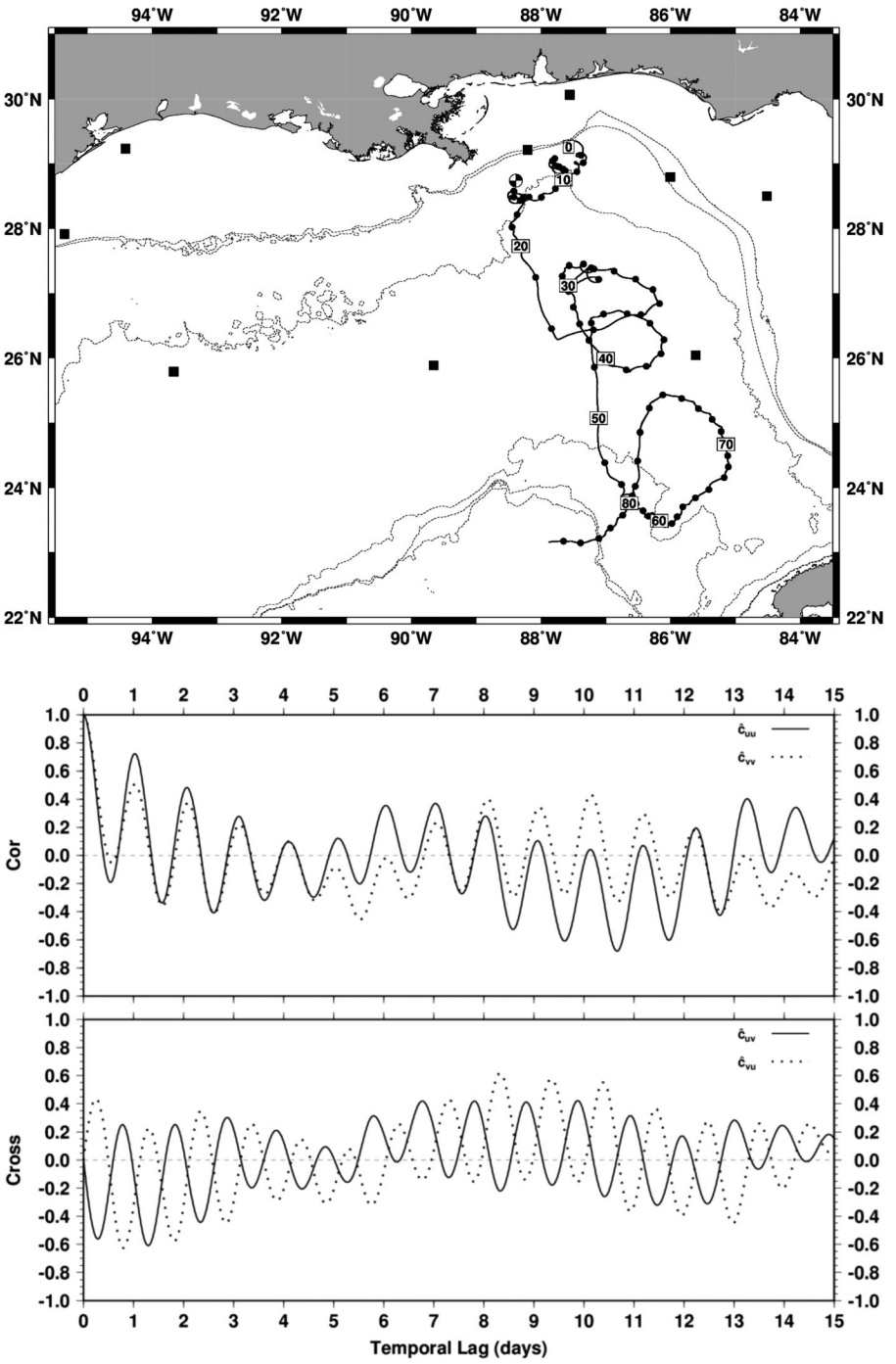

Figure 4. (top) The 85 day trajectory of drifter 218 deployed on 29 July 2012 near the shelf break. It sampled different dynamical regimes from slow flow dominated by inertial motion near the shelf break to faster mesoscale flow in the deeper Gulf of Mexico. The dots are plotted daily, and the number denotes days since deployment. The 200 m, 300 m, and 2000 m isobath contours are also plotted. The 9 black squares are the locations of the National Data Buoy Center (NDBC) moored stations. The Deepwater Horizon site is denoted by the black-white circle. Below the trajectory plots are the (middle) horizontal velocity autocorrelation and (bottom) cross correlation functions for two different 30 day segments for u and v. Drifter 218 velocity autocorrelation and crosscorrelation are calculated for the first 30 days of the trajectory in the middle plot, while the bottom plot is for the last 30 days of the trajectory. The solid and dotted lines in the upper part of the middle and bottom plots are $\hat{C}_{uu}$ and $\hat{C}_{vv}$, respectively. The solid and dotted lines in the lower part of these plots are $\hat{C}_{uv}$ and $\hat{C}_{vu}$, respectively.

A least-squares fit of a linear, temporal trend to each data segment is used for calculating the expected value of u and v for the following reasons. First, the drifters sampled different dynamical regimes and experienced different wind forcing during the 31 day time segments, so their velocity statistics are not constant.

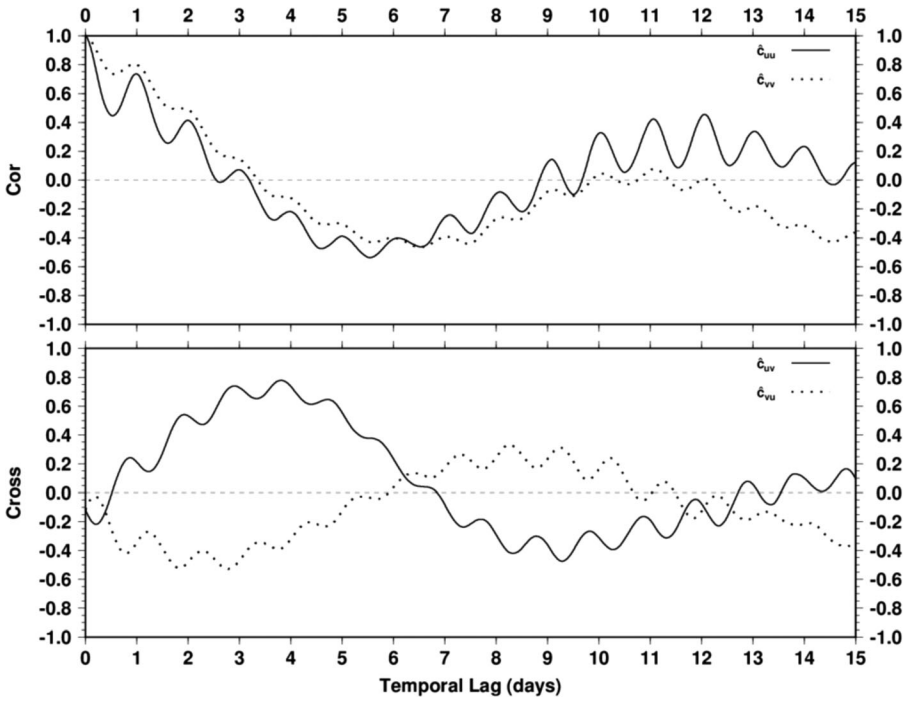

Figure 4. (continued)

Second, the method has already been used and successfully tested in *Garraffo et al*. [2001], with an extensive analysis of both real and simulated trajectories. Finally, there are more statistical outliers in the estimated correlation parameters when using the simple arithmetic average as the mean.

The correlation parameters are estimated from $\hat{C}(\tau_k)$ for each drifter and for each time segment using the contour analysis approach [*Mariano and Chin*, 1996]: $\hat{a}_1$ is the estimated correlation at zero lag whose value is determined by subgrid-scale variability; $\hat{a}_2$ is the dominant period and is estimated by finding the zero-crossing scale, the lag where $\hat{C}(\tau_k)$ is zero, and multiplying it by four; $\hat{a}_3$ is first estimated using the lag where $\hat{C}(\tau_k)$ equals $\frac{\hat{a}_1}{e}$ and is then corrected using the $\hat{a}_2$ value. Given the high temporal resolution of the GLAD drifters, that the data are filtered to remove noise for time scales less than 1 h and are resampled to 15 min during preprocessing, $\hat{a}_1$ is estimated to equal one for all data segments.

The estimated statistics for each data segments are placed at the arithmetic average of the positions for that segment (Figure 1, bottom). These spatial estimates are smoothed and interpolated using bicubic smoothing splines [*Inoue*, 1986] to produce spatial maps. Standard deviations of all the estimated quantities are calculated for each data segment and are used as weights for the smoothing splines. The tensions of the splines are set high in order to allow reliable extrapolation in relatively data-sparse regions [*Inoue*, 1986]. The estimates at the boundary of the maps and in the regions with the lowest data density have the largest mapping error, and the trends at the boundaries may not be significant.

4. Results

GLAD drifter 218 exemplifies a drifter that traveled from the shelf break into the deeper GoM and sampled different dynamical features. Deployed on 29 July, it was slowly advected to the southwest with very strong inertial motion evident in the trajectory during the first 19 days and in the velocity cross-correlations that contain a strong oscillatory signal with a 1 day period (Figure 4). After day 20, the drifter was located in a cyclonic eddy, and by day 49 it ended up in a strong jet near 87°W and 26°N (Figures 2 and 3). Also evident in this trajectory is the increased inertial motion between days 30 and 33 due to Hurricane Isaac, that made landfall on 29 August, day 31, at Port Furchon, Louisiana. The horizontal velocity autocorrelation and cross-correlation functions for the first and last 30 day segments indicate strong nonstationary statistical behavior. Many of the GLAD drifters had similar looking autocorrelation and cross-correlation functions. Different

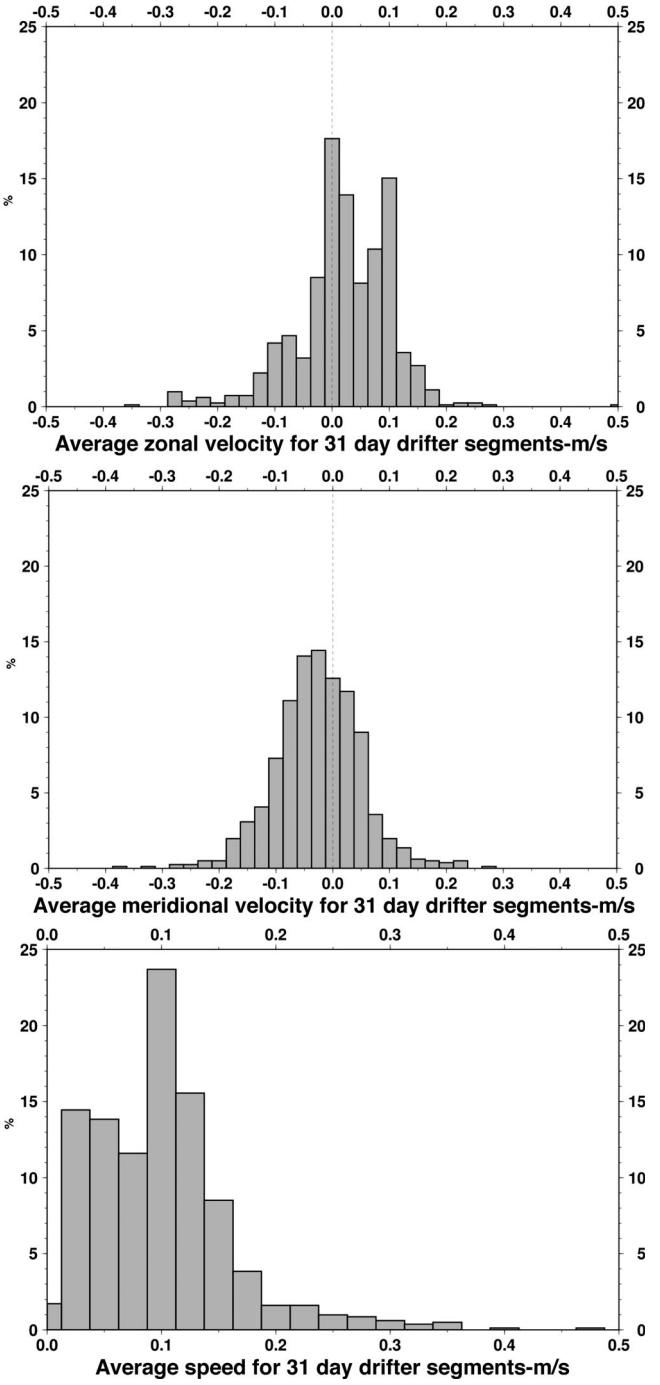

Figure 5. Histograms of the 31 day average (top) u, (middle) v velocity components, and (bottom) speed for all samples in m/s. The vertical axis is the percentage of samples in each bin.

Lagrangian velocity correlation statistics for the different monthly data segments are observed in most of the GLAD drifters due to sampling of different dynamical regimes as well as the temporal variations induced by large changes in wind forcing.

4.1. Observed Flow and Its Variability

The dominant surface flows include inertial motion, tides, submesoscale eddies, a strong southerly jet, shelf waves, and mesoscale cyclonic and anticyclonic eddies. The Loop Current was in its southern mode [*Schmitz*, 2005] with most of its flow from the Yucatan Current directly feeding the Florida Current north of Cuba in the Florida Straits. The flows sampled by the GLAD drifters varied significantly over the region with slow flows near the shelf; energetic cyclonic (anticlockwise-rotating) and anticyclonic (clockwise-rotating) eddies, and a strong southward jet (Figures 2 and 3). Many of the drifters were entrained into the jet or one of the eddies. The jet is observed directly by drifters and indirectly in satellite images [*Berta et al.*, 2015] between 88° W and 87° W and between 23° N and 27° N. The jet was found between the eastern edge of a recently detached anticyclonic Loop Current Eddy and the western edges of two cyclonic eddies that were primarily east of 87° W. The jet constitutes a very efficient path connecting northern GoM water to the waters of the Yucatan shelf. The interactions between these eddies produced strong flow bifurcations near 24° N, 87° W (E in Figure 3), and 26.5° N, 87.5° W (B in Figure 3). The northern cyclone interacted with a weak inshore anticyclonic eddy producing another flow bifurcation near 28° N, 86.5° W (A in Figure 3). The southern cyclone interacted with the Loop Current producing flow bifurcation near 23° N, 86° W (F in Figure 3). Unpredictable Lagrangian motion, large velocity variance, and large velocity shear were observed at the flow bifurcations. The location of the bifurcation points change with time and exact determination is not trivial, so the locations given are approximate, nominal locations. It should be noted that most of the westward flow in the velocity maps (Figures 2 and 3) west of 89° W results from interpolating just ten drifters (Figure 1) that span about 700 km in latitude.

Histograms of the 31 day average velocity estimates for all drifters and overlapping time segments were calculated for both velocity components and for speed (Figure 5). The histograms would probably be different

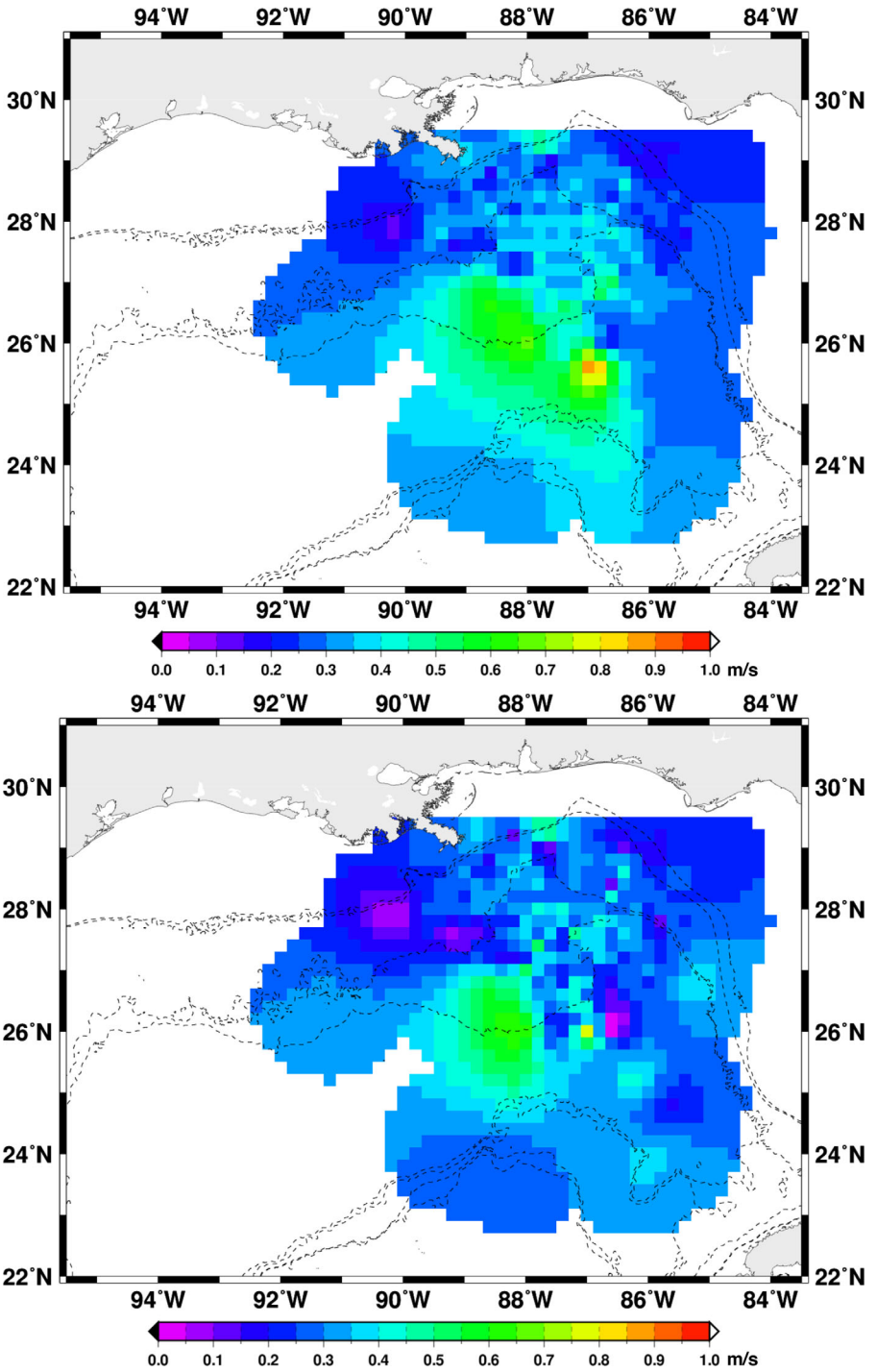

Figure 6. Maps of the (top) u and (bottom) v standard deviation in m/s for the GLAD drifters.

for a different experiment, especially at another time of the year, and that the histograms would have larger variance if the averaging interval is reduced. Typical average speeds were 5–10 cm/s corresponding to a mean transport on the order of 100–200 km/month. Faster average speeds (30–50 cm/s) were calculated for about 7% of the 31 day data segments, all in the deeper waters of the GoM. The *v* histogram is more symmetric and Gaussian-like than the *u* histogram, which exhibits bimodal behavior. There is a net southward movement of the drifters on the order of 5 *cm/s* because of the contribution from the strong southward jet sampled by the GLAD drifters, and a smaller contribution due to the influences of the Mississippi

River outflow, and Ekman transport from the observed winds, from nearby NDBC buoys, that had a mean westerly (winds blowing from west to east) component during the experiment. The secondary peak at 10 *cm/s* in the *u* histogram is due to the large number of drifters that sampled the flow denoted by B-C-D in Figure 3, while the smaller peak at −10 cm/s is due to a smaller number of floats sampling the flow west of E in Figure 3.

The maps of standard deviations of the velocity components (Figure 6) broadly show larger values in deeper water than in the coastal regions. Peaks in standard deviation, which exceed the typical values by almost a full order of magnitude, are associated with the strong mesoscale eddies. Lagrangian Stochastic Models (LSMs) [*Griffa*, 1996; *Piterbarg et al*., 2007], that are used to represent unresolved scales for predictions of particle motion in a fluid, will need to account for this difference in velocity variance in order to achieve the most accurate representation of subgrid scale variability [*Ohlmann et al*., 2012].

4.2. Dominant Period and *e*-Folding Scales

The histograms of the dominant periods (a_2 in equation (1)) for both *u* and *v* are multimodal (Figure 7). The estimates cluster around 1–2 days, 5–6 days, 9–10 days, 13–14 days and longer. *Anderson and Sharma* [2008] analyzed GPS-tracked drifters in the northern GoM and found strong inertial motion with inertial periods ranging from 1 day at 30° N to almost 1.5 days at 20° N. Their estimated near-inertial variance reached a maximum in June, and was strongest during the summer when the mixed layer is the shallowest. *Ohlmann and Niiler* [2005] found a dominant period of 5–10 days for the surface velocity field based on an EOF analysis of the SCULP drifters in this region. They concluded that this period is due to 5–10 day fluctuations in the wind field that result from the passage of synoptic weather events. They found the strongest coherence between their measured currents and the observed winds at a period of 5–6 days. On the other hand, a quick calculation shows that a submesoscale eddy with an azimuthal speed of 0.2 m/s and a radius of 15 km has a 5 day rotational period. This region contains energetic submesoscale eddies. Dominant periods between 8 and 16 days can also be associated with the rotational period of energetic mesoscale eddies that populate this region and were sampled by the GLAD drifters. The dominant period observed by an individual drifter is determined by the particular dynamical feature it sampled. The nature of the dynamical features changes between near-coastal regions inshore and along the shelf-break, and the deeper GoM.

The same correlation parameter estimation method was applied to hourly wind data from nine NDBC stations in the northern GoM for the same time period as sampled by GLAD drifters (Figure 4). There is only one station that exhibits a 1 day dominant period (for the zonal winds), presumable forced by the sea breeze. This station is the closest to land near 94.5° W, 29° N (Figure 4). The other NDBC stations are too far from the coast to see a strong sea breeze signal. Our analysis indicates some correspondence between the ocean surface velocity field and the wind's dominant periods between 5 and 16 days. Based on the analysis of GLAD drifters and other analyses [e.g., *LaCasce and Ohlmann*, 2003; *Ohlmann and Niiler*, 2005; *Anderson and Sharma*, 2008] the 1–2 day dominant period can be associated with inertial oscillations, tides, and sea breeze. Wind forcing and submesoscale motion can explain the 5–6 day dominant period. The 9–10 day period, the two-week period, and longer periods are consistent with both mesoscale variability, including the period of eddy rotation, and with the wind forcing.

The temporal *e*-folding scales for *u* and *v* are more bimodal with shorter time scales of 0.25–0.50 days and of 0.9–1.4 days (Figure 8), corresponding to short time scales that are submesoscale. *Ohlmann and Niiler* [2005] also found the dominant *e*-folding scales of less than 2 days in the northern GoM. The dominant *e*-folding periods for the winds vary between a few hours and less than 2 days, and some are anisotropic with smaller values for the zonal component (Figure 8). The *e*-folding scales for the zonal winds have a fairly uniform distribution while the meridional wind's *e*-folding scale distribution is peaked at 1 day. There is some limited correspondence between the estimated *e*-folding scales for the ocean surface velocity field and for the observed winds. Thus, both sets of correlation parameters, as well as the EOF analysis of *Ohlmann and Niiler* [2005], suggest the importance of synoptic scale wind forcing to the Lagrangian velocity statistics of the surface ocean. On the other hand, an analysis of the spatial maps of statistical properties of the surface velocity field presented next, clearly shows the importance of topography for the flow statistics. Also, the observed anisotropy in the *e*-folding scales of *u* and *v* is different between the ocean currents and the wind, with larger zonal scales in the ocean that are closely aligned with the topography.

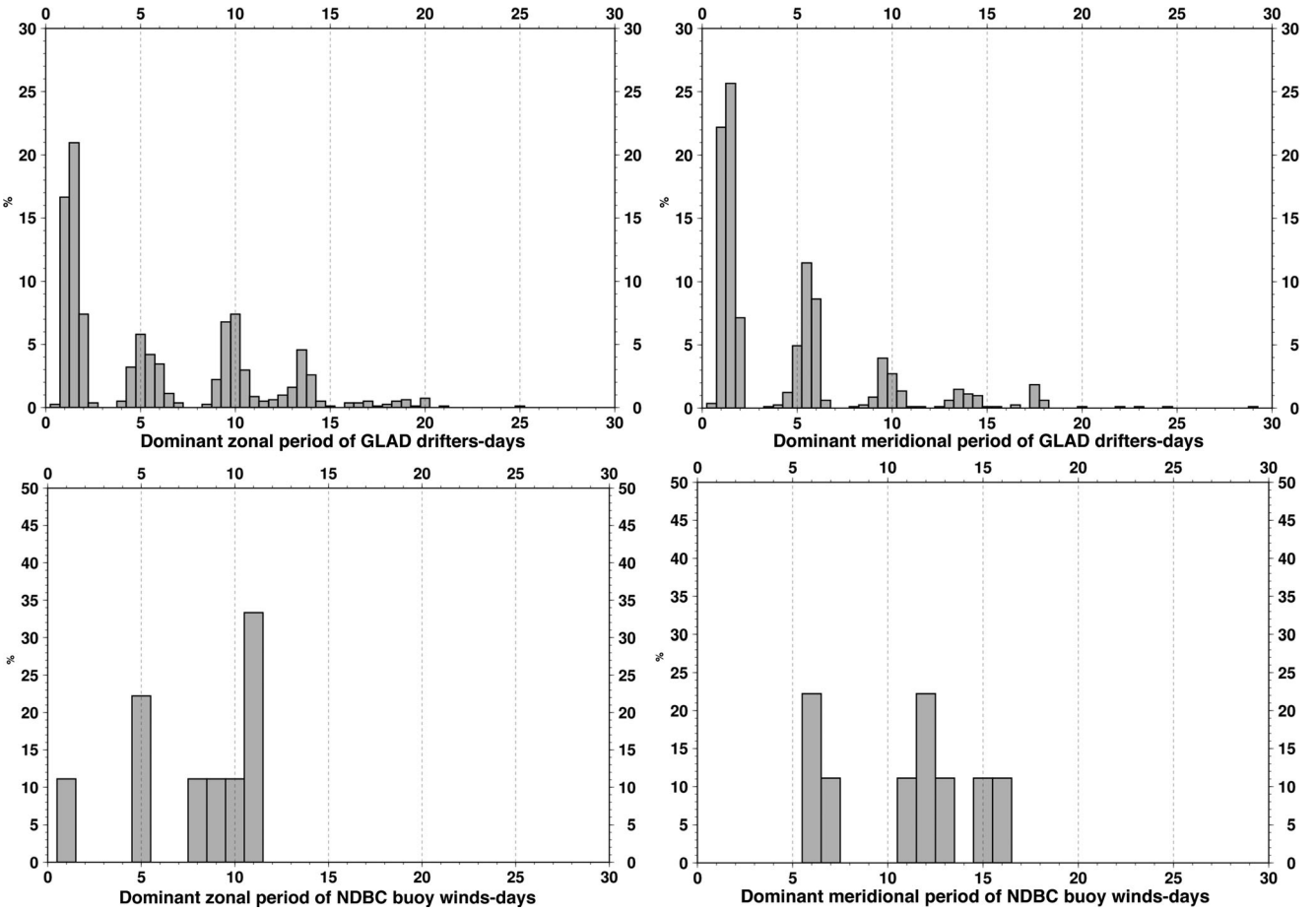

Figure 7. (top) The histograms of the dominant period, in days, of the (left) u and (right) v velocity components for all estimates calculated from the GLAD drifters. The vertical axis is the percentage of samples in each bin. (bottom) The histograms of the 10 m (left) zonal and (right) meridional wind velocity components dominant period calculated for 9 NDBC wind data sets for the same time period.

The *u* and *v* correlation parameter estimates were smoothed and interpolated by bicubic splines, and then combined into ellipses (Figure 9). It should be noted that there is less data (Figure 1, bottom) near the boundaries of all the maps, and the estimated parameters there are noisier than the estimates close to the deployment areas. The spatial maps of the *u* and *v* dominant periods and *e*-folding scales all exhibit the same general trend of increasing time scales from coastal to deep sea waters. The largest anisotropic behavior, exemplified by elongated ellipses in Figure 9, in the *e*-folding ellipses is in the region, 88° W to 87° W, 25.5° N to 27° N (B in Figure 3) which also exhibits the largest velocity variance (Figure 6) associated with flow bifurcation.The dominant period ellipses are more isotropic, (the ellipses are more circular in Figure 9), than the *e*-folding scales.

4.3. Integral Time Scales, Absolute Dispersion, and Horizontal Diffusivity

The starting point for the study of particle dispersion in a fluid is the seminal paper by *Taylor* [1921] who introduced the integral time scales I_u and I_v for a homogeneous/stationary flow field as the integral of the velocity autocorrelation functions, C_{uu}, and C_{vv}.

$$I_u = \int_0^\infty C_{uu}(\tau)d\tau \tag{3a}$$

$$I_v = \int_0^\infty C_{vv}(\tau)d\tau \tag{3b}$$

A fundamental metric of oceanic dispersion, the horizontal eddy diffusivities, $\mathbf{K_H} = (K_u, K_v)$, are defined as

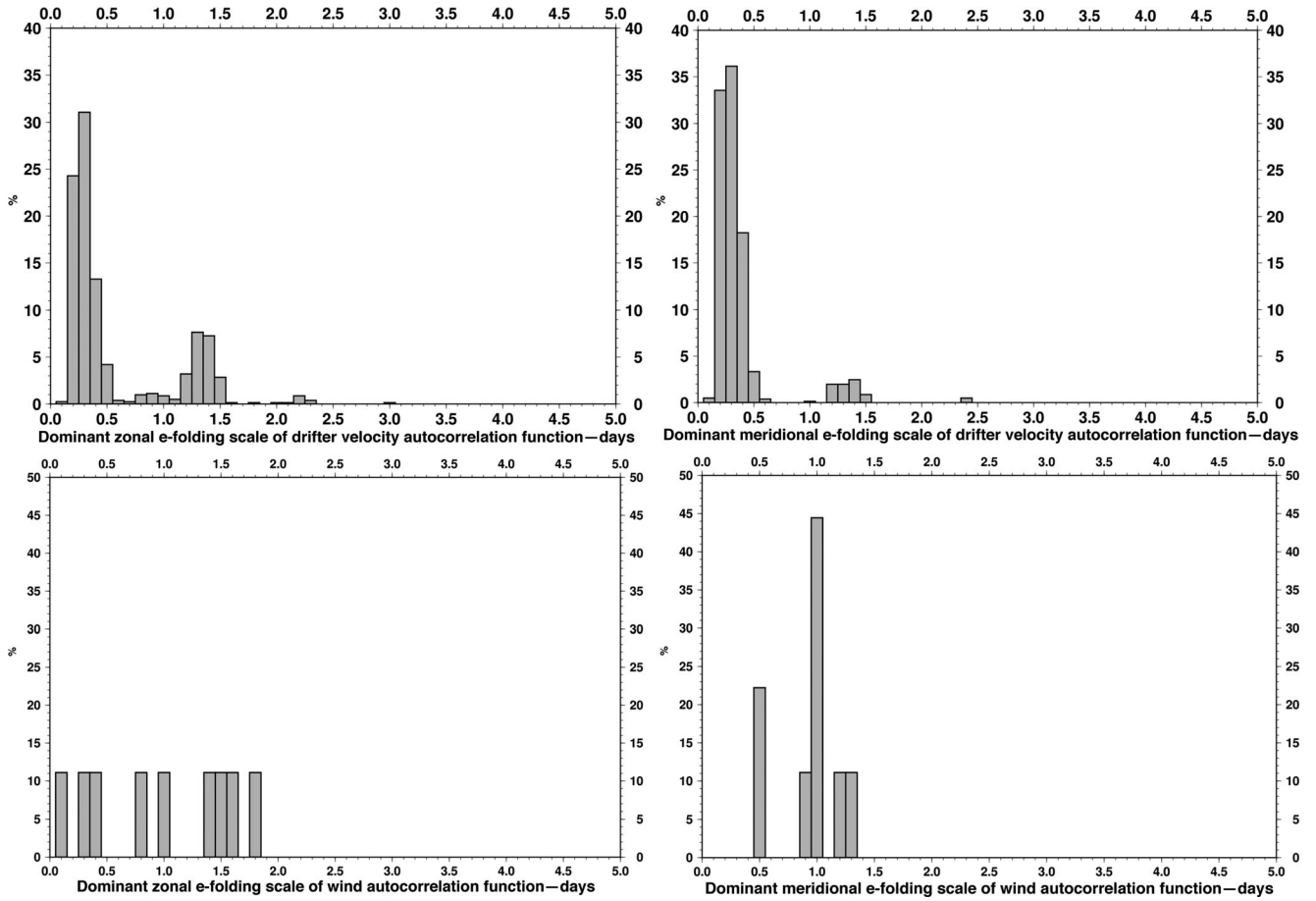

Figure 8. (top) The histograms of the dominant e-folding scales, in days, of the (left) u and (right) v velocity component for all estimates calculated from the GLAD drifters. (bottom) The histograms of the 10 m (left) zonal and (right) meridional wind velocity components dominant e-folding scales, calculated for 9 NDBC wind data sets for the same time. The vertical axis is the percentage of samples in each bin.

$$K_u = \frac{d\,\sigma_X^2(t)}{2\,dt}, \tag{4a}$$

$$K_v = \frac{d\,\sigma_Y^2(t)}{2\,dt}. \tag{4b}$$

The horizontal components of the absolute dispersion, $\sigma_X^2(t)$ and $\sigma_Y^2(t)$, are the variances at time t of the particle position displacement data relative to the deployment position, $(x_i(0), y_i(0))$ for each drifter i calculated by averaging over n drifters in a cluster,

$$\sigma_{\mathbf{X}}^2(t) = \left(\sum_{i=1}^{n} \frac{(x_i(t) - x_i(0))^2}{n-1}, \sum_{i=1}^{n} \frac{(y_i(t) - y_i(0))^2}{n-1} \right). \tag{5}$$

Total horizontal diffusivity is calculated as $K = |\mathbf{K_H}| = \sqrt{K_u^2 + K_v^2}$.

The integral time scales, $\mathbf{I}$, multiplied by the eddy kinetic energy or velocity variance, $\sigma_{\mathbf{V}}^2$, are an estimate of the horizontal eddy diffusivities, $\mathbf{K_H}$, under Taylor's assumptions,

$$K_u = \sigma_u^2 I_u, \tag{6a}$$

$$K_v = \sigma_v^2 I_v. \tag{6b}$$

The square root of the horizontal absolute dispersion $\sigma_{\mathbf{X}} = \sqrt{\sigma_x^2 + \sigma_y^2}$ is expected to grow linearly in time for the time period right after release, and for times greater than twice the integral time scale, the growth in $\sigma_{\mathbf{X}}$ is proportional to the square root of time. These relationships, derived by Taylor, have been observed within

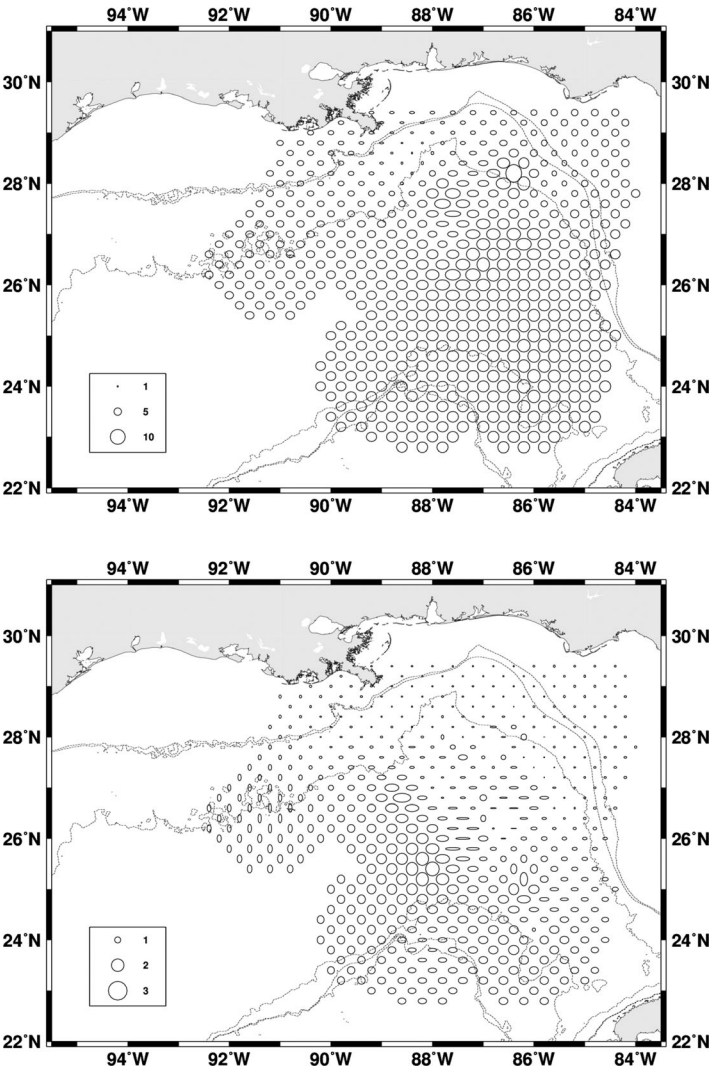

Figure 9. (top) Plot of the dominant period ellipses, in units of days, for both the u and v velocity components. (bottom) Plot of the dominant e-folding scale ellipses, in units of days, for both the u and v velocity components.

estimation error in a number of analyses of Lagrangian ocean data [e.g., *Zhang et al.*, 2001, and references therein], but the simple mean flow and eddy decomposition inherent in Taylor's analyses may not be appropriate for flows with energetic motion across a broad-band of space-time scales or for nonstationary flows [*Riley and Corrsin*, 1974].

Since twice the integral time scale is the time for velocity measurements to become independent, it is fundamental for estimating the effective degree of freedoms in a correlated velocity data set, and for determining for how long a prediction of Lagrangian motion is reliable. Integral time scales and the variance of the velocity field are also used to determine the autoregressive parameters of Lagrangian Stochastic Models (LSMs) [*Griffa*, 1996; *Piterbarg et al.*, 2007] that are used to represent unresolved motion when predicting the motion of a particle in a fluid. A survey of the literature [e.g., *Swenson and Niiler*, 1996; *Zhang et al.*, 2001; *Lumpkin et al.*, 2002; *Bauer et al.*, 2002; *Zhurbas and Oh*, 2003; *Sallée et al.*, 2008; *De Dominicis et al.*, 2012; *Chiswell*, 2013] reveals Lagrangian surface velocity integral time scales on the order of 1 day or shorter in coastal water, and on the order of 2–4 days or more in most of the open ocean, with larger values of 5 days or more associated with strong ocean currents, energetic mesoscale eddies, and the deeper ocean, where the time scales can be on the order of weeks.

The best set of previous estimates of the integral time scales for the northern GoM is from SCULP measurements [*Ohlmann and Niiler*, 2005]. The tracking error is an order of magnitude larger for ARGOS than SPOT. The nominal SCULP drifter temporal sampling rate was 4–6 fixes per day, and 15 drifters were deployed within a 125 km^2 region every week or longer. From these drifters *Ohlmann and Niiler* [2005] estimated integral time scales that ranged from 1.1 to 2.8 days depending on the region. The integral time scale for the along-shore component was about twice as large as the integral time scale for the cross-shore component for the shallowest regions along and inshore of the shelf break. The integral time scales were isotropic at the offshore, deeper locations with an average value of 1.4 days.

The Lagrangian surface velocity integral time scales for *u* and *v*, estimated from the GLAD drifters, increase from on and near-shelf values of 8 h to offshore values of primarily around 2 days and peak values at 3–4 days (Figures 10 and 11). These values are consistent with the previous estimates, although they exhibit a

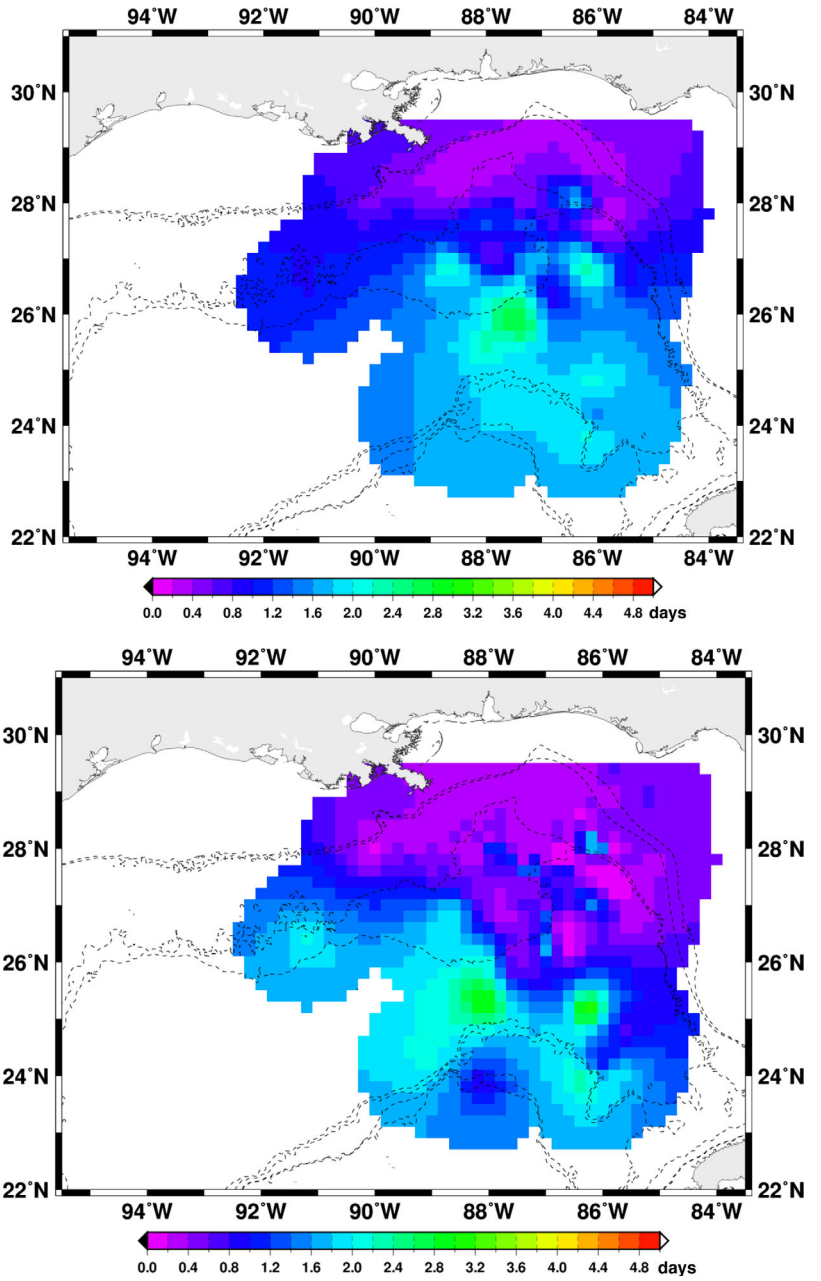

Figure 10. Maps of the integral time scale, in days, of the (top) u and (bottom) v velocity components.

wider range. The integral time scales for both velocity components show a topographic influence with smaller values observed in shallower waters and larger values calculated in the deeper GoM (Figure 10). The spatial maps of the integral time scales for *u* exhibit a sharper gradient offshore of the shelf break than the integral time scales for *v*. We speculate that a possible explanation for this behavior is that the *v* velocity is forced primarily by the large-scale westerly winds in this region via Ekman dynamics, while the *u* velocity is constrained dynamically to satisfy continuity and potential vorticity constraints with a large topographic beta term along the shelf break and in the DeSoto Canyon region. The combined integral time scale amplitudes, $I=\sqrt{I_u^2+I_v^2}$, (Figure 11, bottom) exhibit a local minimum offshore of the shelf break, denoted by the 200 m and 300 m isobaths in the DeSoto Canyon region, indicating relatively slow dispersion. Local maxima in the integral time scales are found in the core of the strong eddies, in the strong jet, and associated with the fast flow on the eastern boundary of the Loop Current Eddy and on the western side of the southern

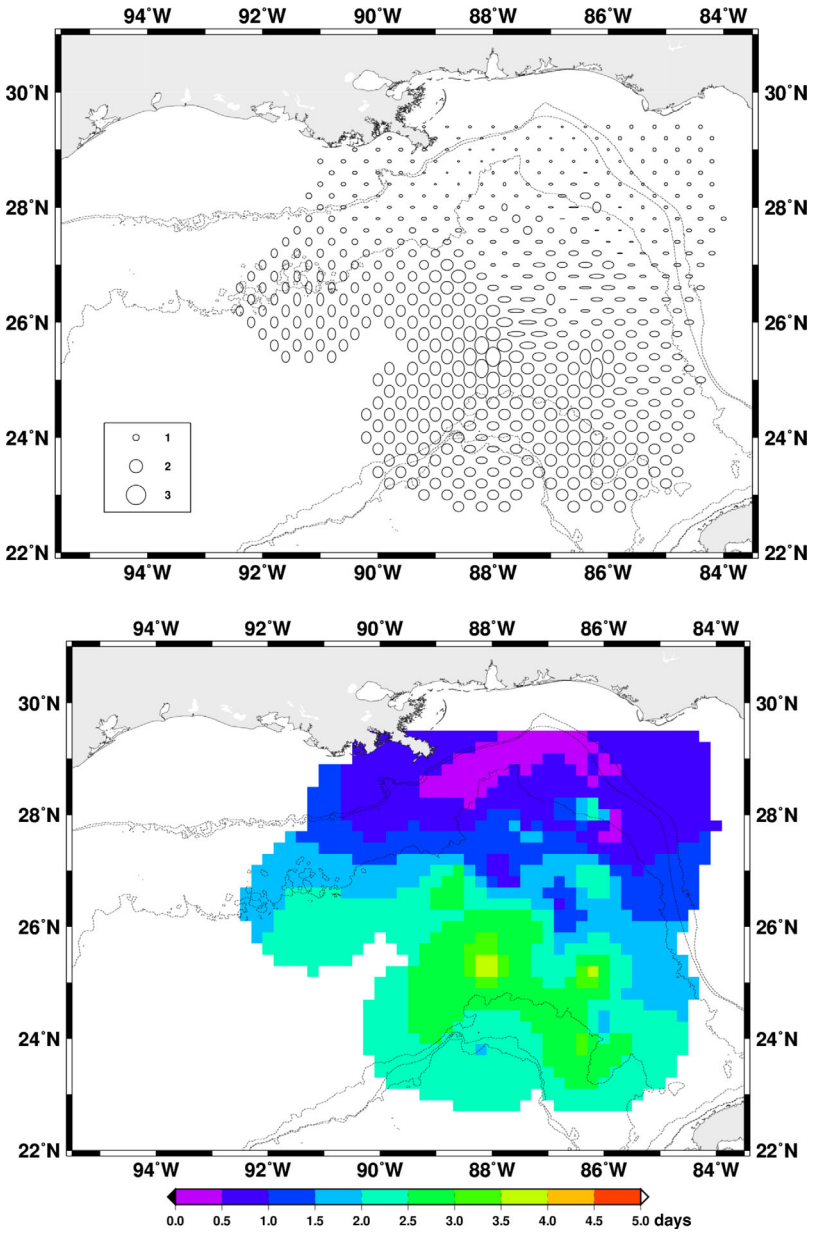

Figure 11. (top) A map of the ellipses of the integral time scale, in days, for the surface velocity field in the northern Gulf of Mexico. (bottom) The amplitude of the integral time scales, $I = \sqrt{I_u^2 + I_v^2}$. Units are days.

cyclone. Besides the local minima in the quiet zones and the local maxima in the energetic features, the integral time scale ellipses (Figure 11, top) are fairly isotropic with anisotropies mainly occurring in the fast flow regions at the edges of mesoscale eddies.

Anisotropic integral time scale values are generally associated with the longitudinal correlation function of the velocity field. *Freeland et al.* [1975] first showed that the scales of the Lagrangian velocity longitudinal correlation function are larger than the transverse correlation function in the ocean, a theoretical result for horizontally nondivergent fluid flow. *Ohlmann and Niiler* [2005] observed anisotropic integral time scales for surface drifters on and near the shelf in the northern GoM, in wind-driven flows steered by the topography. In contrast, GLAD's estimated anisotropic integral time scale values (Figure 11) are primarily at the same locations as the anisotropic temporal *e*-folding scales (Figure 9) that are associated with flow bifurcations. The *e*-folding scales are set by the broad-band turbulence of the

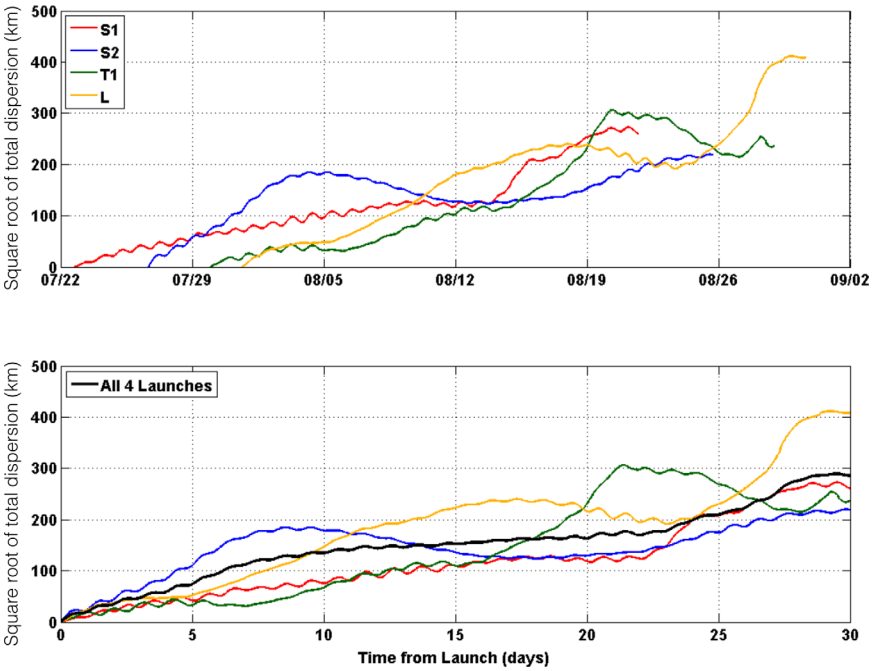

Figure 12. (top) The square root of the absolute dispersion, in units of km, of the four major launches, each denoted by a different color, as a function of launch date. (bottom) Same as the top plot but as a function of days after launch. The bottom plot also shows the square root of absolute dispersion for all drifters in black. The effects of Hurricane Isaac that was in the area 27–29 August is evident in the absolute dispersion estimates.

northern GoM observed by GLAD drifters, as is detailed in *Poje et al*. [2014], and are more anisotropic near flow bifurcations.

The square root of the absolute dispersion was calculated for the four primary subsets of the GLAD drifters (Figure 12). S1 and S2 were the two multiscale deployments of 10 clusters of 9 drifters along an S-shaped ship track near the well site. The T deployment consisted of 27 drifters at the Northern tip of the DeSoto Canyon deployed along a triangular ship track. The L deployment consisted of 60 drifters in two L-shaped patterns targeting a cyclonic eddy. The effects of both flow bifurcations and Hurricane Isaac primarily caused these four deployment clusters to disperse widely after 1 month, limiting the dispersion calculation. The four different estimates of absolute dispersion all contain a strong diurnal signal, and different amounts of eddy dispersion effects on the longer time scales.

The square root of the absolute dispersion estimates varied by a factor of 2–4 a few days after launch due to the heterogeneity of the surface flow dynamics sampled by the GLAD drifters. The average square root of the absolute dispersion curve, calculated by averaging the estimates from the four data subsets for each day after deployment (black curve in Figure 12), contained an inertial component superimposed on a linear trend for the first week followed by a more gradual trend. A linear trend was expected for flow obeying *Taylor*'s assumption. The slopes of the average square root of the absolute dispersion curve start to decrease after the first week after launch as theory suggests. After that time, between 27 and 29 August, Hurricane Isaac went right over many of the drifters. Hurricane Isaac's strong winds significantly changed the surface velocity statistics, increased dispersion over a large area, caused drifters to be beached in the Mississippi Delta region, and were responsible for a premature termination of some drifters. *Curcic et al*. [2016] detail the significant changes due to Isaac in the upper ocean flow and wave fields, including increasing relative diffusivity by a factor of six.

K is directly calculated using (4a) and (4b) for the primary drifter clusters for the first month of the deployment by fitting a tense cubic spline to the time series of the position variance divided by 2, and calculating the temporal derivative from the spline fit (curves in Figure 13). There is a lot of variability in the estimates of K with its magnitude varying by three orders of magnitude. The largest diffusivity values are $O(10^5)$ m^2/s with the maximum occurring at the time of Hurricane Isaac, and the largest values associated with drifters

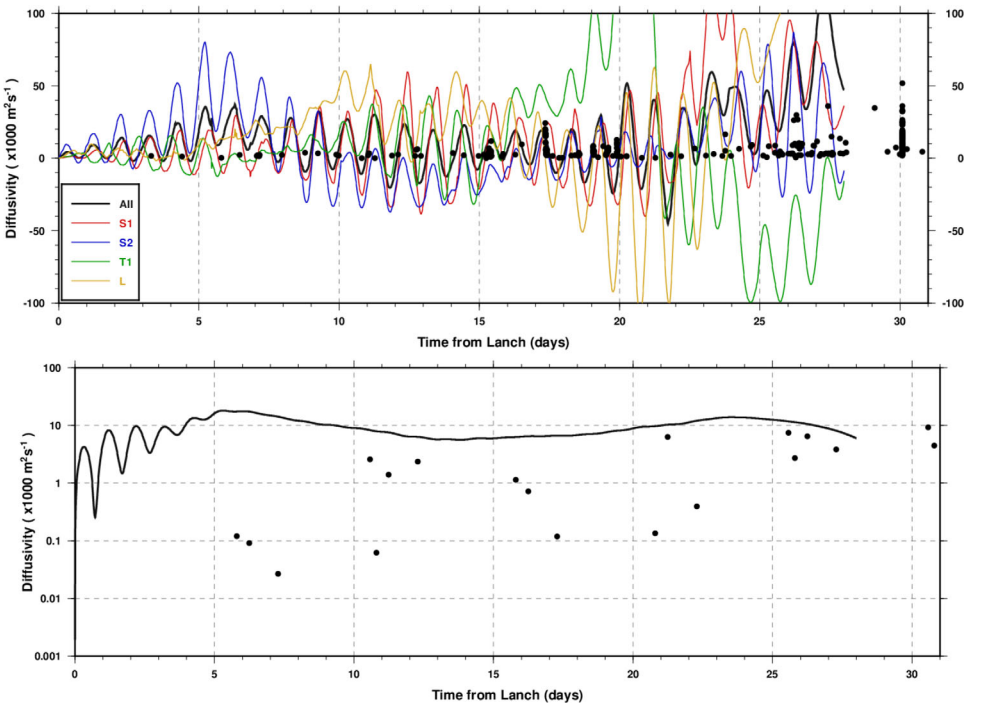

Figure 13. (top) The horizontal diffusivity K, in 10^3 m^2/s, as a function of time after deployment in days for the primary drifter clusters. Note that the smallest and largest values fall outside the axis limits here. The minimum and maximum values of K are from cluster L and are -110×10^3 m^2/s and 360×10^3 m^2/s, respectively. The dots show the horizontal diffusivity calculated by Taylor's method as described in the text. (bottom) The solid line in this plot is a spline-smoothed version of the ALL curve from the top figure on a log scale. The dots are an average of all of the Taylor-based estimates for each of the temporal midpoints of the 31 day data segments.

in the jet and the Loop Current Eddy. Negative values of *K* are presumably due to inertial motion and eddies that cause drifters to get closer to their initial positions. The temporal trend of increasing *K* is due to more drifters entering the energetic eddy flows in the deeper waters after leaving the shelf. A smoothing spline [*Inoue*, 1986] fit to the average diffusivity time series yields lower estimates of the maximum *K* by an order of magnitude (Figure 13, bottom) with an asymptote of $O(10^4)$ m^2/s.

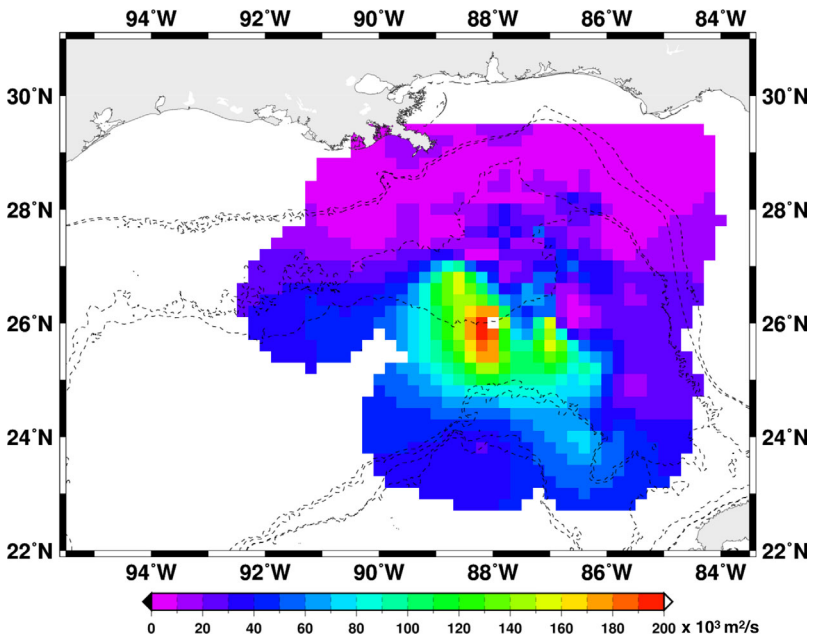

Figure 14. The horizontal diffusivity, in 10^3 m^2/s, based on the integral time scales, velocity variance, and Taylor's analyses.

Table 1. Previous Diffusivity Estimates for Near-Surface Drifters

Diffusivity -(m^2/s)	Region	Reference
6.4×10^2	Near-coast Louisiana-Texas Shelf	*Ohlmann and Niiler* [2005]
2.1×10^3	Louisiana-Texas Mid-Shelf	*Ohlmann and Niiler* [2005]
2.2×10^3	Louisiana-Texas 200 m isobath	*Ohlmann and Niiler* [2005]
$1.5-3.0\times10^3$	Ligurian Sea and Adriatic Sea	*De Dominicis et al.* [2012]
$3.1-6.4\times10^3$	West Florida Shelf	*Ohlmann and Niiler* [2005]
$O(10^3)$	Antarctic Shelf	*Sallée et al.* [2008]
$O(10^4)$	Antarctic Circumpolar Current	*Sallée et al.* [2008]
$O(10^3)-O(10^4)$	Global Near-surface	*Zhurbas and Oh* [2004]
$O(10^3)-O(10^5)$	Tropical Pacific	*Bauer et al.* [2002]
$O(10^3)-O(10^5)$	Tropical Pacific and Indian Ocean	*Chiswell* [2013]

Diffusivity estimates based on (6) for the different data segments also show considerable variations, and that most of the Taylor-based estimates are between 10^3 and 10^4 m^2/s for the first month of deployment (black dots in Figure 13). Estimates of this quantity from the GLAD drifters vary by two orders of magnitude from the coastal regions with weaker flow to the stronger flows, in deeper waters, with values ranging from $O(1\times10^3\ m^2/s)$ to $O(2\times10^5\ m^2/s)$ (Figure 14). The estimates of K using Taylor's results in the same figure are averages of all Taylor-based diffusivity estimates in Figure 13, top, for each of the temporal midpoints of the data segments for each cluster during the first month of the experiment. The Taylor estimates are lower presumably due to the compounded averaging, which is a smoothing operation. The direct estimates of total horizontal diffusivity are based on calculating a derivative, an operation that is not smoothing. *Chiswell* [2013] also found that Taylor-based diffusivity estimates are lower than those directly estimated from taking temporal derivatives. The variability and sensitivity of the K estimates even for such a large data set indicate that the simple dispersion theories postulating a uniform K value are not applicable for surface flow in this dynamically diverse region.

GLAD horizontal diffusivity estimates span the same two orders of magnitude as the previous diffusivity estimates for near-surface drifters (Table 1). The lowest horizontal diffusivity values, $O(10^3\ m^2/s)$, in all of these studies are found near the coast and shelf. The largest diffusivity values, in the previous studies, are found in regions with strong flows and large values of eddy kinetic energy. *Sallée et al*. [2008] estimated their largest diffusivity value where the Antarctic Circumpolar Current interacts with topography and *Bauer et al*.'s [2002] largest estimates are in the core of the South Equatorial Current. The largest diffusivity value estimated for GLAD drifters is $O(2\times10^5\ m^2/s)$ compared to $O(10^5\ m^2/s)$ diffusivity values estimated by *Bauer et al*. [2002] and *Chiswell* [2013].

The GLAD diffusivity estimates agree with previous estimates of diffusivity near and along the shelf, and in most of the deeper GoM. Our analysis of the GLAD drifters also produced a similar trend of smaller integral time scales and diffusivity values near the coast increasing to larger values in the deeper GoM. The most significant difference between the GLAD and previous diffusivity estimates is that our maximum estimates are larger than previous estimates. The larger diffusivity values are found in the region of fastest flow where there is significant velocity shear and flow bifurcations, and during Hurricane Isaac. *Davis* [1987], *Bauer et al*. [1998], *Oh et al*. [2000], and *Zhurbas and Oh* [2004] discuss methods to reduce the contribution of horizontal velocity shear to dispersion. On the other hand, the large diffusivity estimates are large where they should be large, at strong flows with bifurcation points that are fully resolved by the GLAD drifters, and it is well known that climatological averages of geophysical variables are biased low [*Mariano and Chin*, 1996]. It should be noted that this large diffusivity would be appropriate for mean velocity fields that do not resolve the flow bifurcations, but would be an over-estimate (positive bias) for an accurate and highly resolved set of mean velocity fields that contain the flow bifurcations.

A cluster of drifters will diffuse up a gradient of eddy diffusivity with an induced velocity $\mathbf{V_i}$ [*Freeland et al*., 1975],

$$\mathbf{V_i}=(u_i,v_i)=\left\langle \frac{\partial K_u}{\partial x},\frac{\partial K_v}{\partial y}\right\rangle.$$

The up-gradient flux is on the order of 2 *cm/s* for v_i for the large meridional gradient in K_v (Figure 14).

5. Conclusions

In summary, the large volume and high resolution of data generated by the GLAD drifters allowed reliable estimation and mapping of the average velocity and its variance, correlation parameters, and integral time

scales in the northern GoM during the summer of 2012. Spatial maps of our estimates clearly demonstrate a strong dependency of the primary surface velocity statistics on topography, and on the location of flow bifurcations. Likewise, the statistical properties of the surface velocity are clearly a strong function of the dynamical feature sampled and of the wind forcing. The dependency of Lagrangian statistics on initial flow conditions has been well-known for many decades, e.g., from the lab studies of *Welander* [1955], the calculations by *Flierl* [1981] for simple but realistic ocean flows, for textbook flows with an energetic high-frequency component [*Aref*, 1984], and for the quasi-Lagrangian ocean measurements reviewed in the LAPCOD book [*Griffa et al*., 2007]. The initial flow conditions are a function of the dynamical features sampled, which vary in the northern GoM due to topography, wind forcing, and proximity to the Loop Current. Also, strong wind forcing quickly changes the surface velocity statistics. The observed GLAD statistics are nonstationary.

As the nature of the dynamics changes from coastal to oceanic, so do the statistical properties of the surface velocity in the northern GoM. There are large changes in the statistical properties for all of the derived statistical quantities with smaller values near the coast and larger values in the deeper waters. The strong inertial, tidal, diurnal wind-forced motion, and submesoscale eddy features in this region are significant sources of high frequency variability. The surface velocity statistics are influenced by strong forcing as evident in the passage of Hurricane Isaac through the area. Thus, all of the necessary conditions for heterogeneous and nonstationary statistics exist in the northern GoM. The histograms for most of the statistical parameters are multimodal and also change depending on the dynamical features sampled. The multimodal distribution of the e-folding scales and dominant period, as well as the spatio-temporal distribution of the velocity variance estimates lead to a family of surface velocity covariance functions. The assumption of a single uniform distribution prior in Bayesian-based analysis or the use of a single covariance function for assimilation methods is not optimal for the surface velocity field of this region. A method analogous to the parameter matrix algorithm of *Mariano and Brown* [1992] will be required with parameter values increasing offshore.

Taylor's results depend on stationary velocity statistics, but such statistics do not exist in the surface velocity field of the northern GoM. Taylor's results relating diffusivities to integral time scales were derived assuming stationary velocity statistics. Nevertheless, Taylor-based estimates can provide order of magnitude estimates of diffusivity. It must be noted that these estimates and any climatological estimates are of little use for operational, real-time prediction of oil movement, given that K is a strong function of dynamical features and of the wind forcing. The dependency of K and the probability density distribution of the statistical parameters on dynamical features will be a challenging task for numerical modelers and data assimilation algorithms to incorporate into Eulerian models.

The maximum diffusivity values for the GLAD drifters that are calculated either directly or using Taylor's analyses are larger by an order of magnitude than most climatological diffusivity estimates for surface flows, and a factor of two greater than previous maximum estimates. These large values are associated with a jet, that results from the interaction of a Loop Current eddy and cyclonic eddies, adequately sampled by the GLAD drifters, and are a "snapshot" compared to climatological averages. The largest diffusivity was estimated during the passage of Hurricane Isaac in the vicinity of flow bifurcations. Outside of the large diffusivity region near 88−87° W, 26° N, the GLAD diffusivity estimates also exhibit a visual correlation with topography. There is a large topographic beta in this region and its influence on the fluid dynamics, and hence the integral time scales and diffusivities, should be large.

GLAD is a major step in understanding the spatial distribution of the surface velocity statistics in the northern GoM and should be repeated at other times of the year to investigate the stationarity of the velocity statistics with respect to the seasons and to different atmospheric forcing. It should be stressed for management purposes that the region of the 2010 oil spill in the GoM has relatively weak flow and low diffusivity values. Also, the super-positioning of strong dynamical features can lead to long distance transport pathways across climatological mean velocity fields. GLAD drifters sampled such a pathway and verified their efficient transport properties first deduced from satellite images of ocean color and numerical model simulations [*Toner et al*., 2003]. The rapid advection of drifters via this pathway quickly brought drifters into a different dynamical regime with different surface velocity statistics to sample.

The large spatio-temporal variability in the observed velocity statistics, and in diffusivity estimates, indicates that classical theory, while elegant in the mathematical world, does not adequately describe the real world.

The ergodic theorem that allows us to replace ensemble averages of different flow realizations by a large number of data points is the starting point for the analysis of geophysical data. The GLAD experiment shows that even with 5 million data points only a few energetic eddies were primarily sampled, and that the velocity statistics are a strong function of the dynamical feature sampled. Oceanographers necessarily can only sample one realization of the flow for any given space-time volume of strongly varying ocean dynamics and consequently need to be wary of making the ergodic assumption. The dispersion statistics computed from the GLAD drifter data set suggest that a new paradigm is needed for ocean dispersion that does not depend on stationary flow in homogeneous domains, but accounts for different dynamical features and their interactions.

Acknowledgments

This research was made possible by a grant from The Gulf of Mexico Research Initiative. Data are publicly available through the Gulf of Mexico Research Initiative Information & Data Cooperative (GRIIDC) at https://data.gulfresearchinitiative.org (doi:<10.7266/N7VD6WC8>). The GLAD experiment would not have been possible without the hard work of many people including Captain Shawn Lake and the crew of the R/V Walton Smith, the U. of Miami marine technology group, and especially Mike Rebozo. The authors gratefully acknowledge and thank two anonymous reviewers for their comments and suggestions. Comments by Andrew Poje on an earlier draft are very much appreciated. This work was also supported by the international collaboration with the ISMAR-CNR, through the EU-MED Project TOSCA (Tracking Oil Spills and Coastal Awareness network), and by NSF grants OCE 0352104 to Mariano and DMS 1109856 to Restrepo.

References

Anderson, S. P., and N. Sharma (2008), Satellite-tracked drifter measurements of inertial currents in the Gulf of Mexico, in *Proceedings of the IEEE/OES/CMTC Ninth Working Conference on Current Measurement Technology*, pp. 285–288, Charleston, S. C., doi:10.1109/CCM.2008.4480882.

Aref, H. (1984), Stirring by chaotic advection, *J. Fluid Mech.*, *143*, 1–21

Bauer, S., M. S. Swenson, A. Griffa, A. J. Mariano, and K. Owens (1998), Eddy-mean decomposition and eddy-diffusivity estimates in the tropical Pacific Ocean, *J. Geophys. Res.*, *103*, 30,855–30,871.

Bauer, S., M. S. Swenson, and A. Griffa (2002), Eddy mean flow decomposition and eddy diffusivity estimates in the tropical Pacific Ocean: 2. Results, *J. Geophys. Res.*, *107*(C10), 3154, doi:10.1029/2000JC000613.

Berta, M., A. Griffa, M. G. Magaldi, T. M. Özgökmen, A. C. Poje, A. C. Haza, and M. J. Olascoaga (2015), Improved surface velocity and trajectory estimates in the Gulf of Mexico from blended satellite altimetry and drifter data, *J. Atmos. Oceanic Technol.*, *32*, 1880–1901, doi:10.1175/JTECH-D-14-00226.1.

Carnes, M. R., W. J. Teague, and E. Jarosz (2008), Low-frequency current variability observed at the shelfbreak in the northeastern Gulf of Mexico: November 2004-May 2005, *Cont. Shelf Res.*, *28*, 399–423.

Chiswell, S. M. (2013), Lagrangian time scales and eddy diffusivity at 1000m compared to the surface in the South Pacific and Indian Oceans, *J. Phys. Oceanogr.*, *43*, 2718–2732.

Coelho, E. F., et al. (2015), Ocean current estimation using a Multi-Model Ensemble Kalman Filter during the Grand Lagrangian Deployment experiment (GLAD), *Ocean Modell.*, *87*, 86–106, ISSN: 1463-5003, doi:10.1016/j.ocemod.2014.11.001.

Curcic, M., S. S. Chen, and T. M. Özgökmen (2016), Hurricane-induced ocean waves and stokes drift and their impacts on surface transport and dispersion in the Gulf of Mexico, *Geophys. Res. Lett.*, *43*, 2773–2781, doi:10.1002/2015GL067619.

Davis, R. E. (1985), Drifter observations of coastal surface currents during CODE: The method and descriptive view, *J. Geophys. Res.*, *90*, 4741–4755.

Davis, R. E. (1987), Modeling eddy transport of passive tracers, *J. Mar. Res.*, *45*, 635–666.

Davis, R. E. (1991), Lagrangian ocean studies, *Annu. Rev. Fluid Mech.*, *23*, 43–64.

De Dominicis, M. G., Leuzzi, P. Monti, N. Pinard, and P. M. Poulain (2012), Eddy diffusivity derived from drifter data for dispersion model applications, *Ocean Dyn.*, *62*(9), 1381–1398, doi:10.1007/s10236-012-0564-2.

DiMarco, S. F., W. D. Nowlin, and R. O. Reid (2005), A Statistical Description of the Velocity Fields from Upper Ocean Drifters in the Gulf of Mexico, in Circulation in the Gulf of Mexico: Observations and Models, edited by W. Sturges and A. Lugo-Fernandez, AGU, Washington, D. C., doi:10.1029/161GM08.

Flierl, G. R. (1981), Particle motions in large amplitude wave fields, *Geophys. Astrophys. Fluid Dyn.*, *18*, 39–74.

Freeland, H. J., P. B. Rhines, and T. Rossby (1975), Statistical observations of the trajectories of neutrally buoyant floats in the North Atlantic, *J. Mar. Res.*, *33*, 383–404.

Garraffo, Z., D. A. J. Mariano, A. Griffa, C. Veneziani, and E. P. Chassignet (2001), Lagrangian data in a high resolution numerical simulation of the North Atlantic. I: Comparison with in-situ float data, *J. Mar. Syst.*, *29*, 157–176.

Griffa, A. (1996), Applications of stochastic particle models to oceanographic problems, in *Stochastic Modelling in Physical Oceanography*, edited by R. Adler, P. Muller, and B. Rozovskii, pp. 113–128, Birkhauser Boston, Cambridge, Mass.

Griffa, A., D. Kirwan, A. J. Mariano, T. M. Özgökmen, and T. Rossby (2007), *Editors of Lagrangian Analysis and Predictability of Coastal and Ocean Dynamics*, Cambridge Univ. Press, N. Y.

Inoue, H. (1986), A least-squares smooth fitting for irregularly spaced data: Finite-element approach using the cubic B-spline basis, *Geophysics*, *51*, 2051–2066.

Jacobs, G. A., et al. (2014), Data assimilation considerations for improved ocean predictability during the Gulf of Mexico Grand Lagrangian Deployment (GLAD), *Ocean Modell.*, *83*, 98–117, ISSN: 1463-5003, doi:10.1016/j.ocemod.2014.09.003.

Klocher, A., R. Ferrari, J. H. LaCasce, and S. T. Merrifield (2012), Reconciling float-based and tracer-based estimates of lateral diffusivities, *J. Mar. Res.*, *70*, 569–602.

LaCasce, J. H., and C. Ohlmann (2003), Relative dispersion at the surface of the Gulf of Mexico, *J. Mar. Res.*, *61*, 285–312.

Lumpkin, R., and G. C. Johnson (2013), Global ocean surface velocities from drifters: Mean, variance, ENSO response, and seasonal cycle, *J. Geophys. Res. Oceans*, *118*, 2992–3006, doi:10.1002/jgrc.20210.

Lumpkin, R., and M. Pazos (2007), Measuring surface currents with Surface Velocity Program drifters: The instrument, its data and some recent results, in *Lagrangian Analysis and Prediction of Coastal and Ocean Dynamics*, edited by A. Griffa et al., chap. 2, pp. 39–67, Cambridge Univ. Press, N. Y.

Lumpkin, R., A.-M. Treguier, and K. Speer (2002), Lagrangian eddy scales in the Northern Atlantic Ocean, *J. Phys. Oceanogr.*, *32*, 2425–2440.

Mariano, A. J., and O. B. Brown (1992), Efficient objective analysis of dynamically heterogeneous and nonstationary fields via the parameter matrix, *Deep Sea Res., Part A*, *39*(7/8), 1255–1271.

Mariano, A. J., and T. M. Chin (1996), Feature and Contour based data analysis and assimilation in physical oceanography, in *Stochastic Modelling in Physical Oceanography*, edited by R. J. Adler, P. Muller and B. L. Rozovskii, pp. 311–342, Birkhauser, Boston, Cambridge, Mass.

Mariano, A. J., V. H. Kourafalou, A. Srinivasan, H. Kang, G. R. Halliwell, E. H. Ryan, and M. Roffer (2011), On the modeling of the 2010 Gulf of Mexico Oil Spill, *Dyn. Atmos. Oceans*, *52*, 322–340, doi:10.1016/j.dynatmoce.2011.06.001.

Oh, I. S., V. Zhurbas, and W. S. Park (2000), Estimating horizontal diffusivity in the East Sea (Sea of Japan) and the northwest Pacific from satellite-tracked data, *J. Geophys. Res.*, *105*, 6483–6492.
Ohlmann, J. C., and P. Niiler (2005), Circulation over the continental shelf in the northern Gulf of Mexico, *Prog. Oceanogr.*, *64*, 45–81.
Ohlmann, J. C., J. H. LaCasce, L. Washburn, A. J. Mariano, and B. Emery (2012), Relative dispersion observations and trajectory modeling in the Santa Barbara Channel, *J. Geophys. Res.*, *117*, C05040, doi:10.1029/2011JC007810.
Olascoaga, M. J., et al. (2013), Drifter motion in the Gulf of Mexico constrained by altimetric Lagrangian coherent structures, *Geophys. Res. Lett.*, *40*, 6171–6175, doi:10.1002/2013GL058624.
Özgökmen, T. M. (2012), CARTHE: GLAD experiment CODE-style drifter trajectories (lowpass filtered, 15 minute interval records), northern Gulf of Mexico near DeSoto Canyon, July-October 2012, *Gulf of Mexico Res. Initiative, 10.7266/N7VD6WC8*. [Available at https://data.gulfresearchinitiative.org/data/R1.x134.073:0004.]
Özgökmen, T. M., et al. (2014), Research Overview of the Consortium for Advanced Research on Transport of Hydrocarbon in the Environment (CARTHE), in *International Oil Spill Conference Proceedings: May 2014*, vol. 2014, *1*, pp. 544–560, Allen Press, Inc. Savannah, Ga.
Piterbarg, L. I., T. M. Özgökmen, A. Griffa, and A. J. Mariano (2007), Predictability of Lagrangian Motion in the Ocean, in *Lagrangian Analysis and Predictability of Coastal and Ocean Dynamics*, edited by A. Griffa et al., pp. 136–172, Cambridge Univ. Press, N. Y.
Poje, A. C., et al. (2014), Submesoscale dispersion in the vicinity of the Deepwater Horizon spill, *Proc. Natl. Acad. Sci. U. S. A.*, *111*(35), 12,693-12,698.
Riley, J. J., and S. Corrsin (1974), The relation of turbulent diffusivities to Lagrangian velocity statistics for the simplest shear flow, *J. Geophys. Res.*, *79*, 1768–1771, doi:10.1029/JC079i012p01768.
Sallée, J. B., K. Speer, R. Morrow, and R. Lumpkin (2008), An estimate of Lagrangian eddy statistics and diffusion in the mixed layer of the Southern Ocean, *J. Mar. Res.*, *66*, 441–463.
Schmitz, W. J. (2005), Cyclones and westward propagation in the shedding of 941 anticyclonic rings from the Loop Current, *Eos Trans. AGU*, *942*, 241–261.
Sturges, W., and K. E. Kenyon (2008), Mean flow in the Gulf of Mexico, *J. Phys. Oceanogr.*, *38*, 1501–1514.
Sturges, W., and A. Lugo-Fernandez (2005), Circulation in the Gulf of Mexico: Observations and models, *AGU Geophys. Monogr. Ser.*, 161, 347 pp., AGU, Washington, D. C.
Swenson, M. S., and P. P. Niiler (1996), Statistical analysis of the surface circulation of the California Current, *J. Geophys. Res.*, *101*, 22,631–22,645.
Taylor, G. I. (1921), Diffusion by continuous movements, *Proc. London Math. Soc.*, *20*, 196–211.
Toner, M., A. D. Kirwan Jr., A. Poje, L. H. Kantha, F. E. Muller-Karger, and C. K. R. T. Jones (2003), Chlorophyll dispersal by eddy-eddy interactions in the Gulf of Mexico, *J. Geophys. Res.*, *108*(C4), 3105, doi:10.1029/2002JC001499.
Welander, P. (1955), Studies on the general development of motion in a two-dimensional, ideal fluid. *Tellus*, *7*, 141–156.
Yaremchuk, M., and E. F. Coelho (2015), Filtering drifter trajectories sampled at submesoscale resolution, *IEEE J. Oceanic Eng.*, *40*(3), 497–505.
Zhang, H.-M., M. D. Prater, and T. Rossby (2001), Isopycnal Lagrangian statistics from the North Atlantic Current RAFOS floats observations, *J. Geophys. Res.*, *106*, 13,817–13,836.
Zhurbas, V., and I. S. Oh (2003), Lateral diffusivity and Lagrangian scales in the Pacific Ocean as derived from drifter data, *J. Geophys. Res.*, *108*(C5), 3141, doi:10.1029/2002JC001596.
Zhurbas, V., and I. S. Oh (2004), Drifter-derived maps of lateral diffusivity in the Pacific and Atlantic Oceans in relation to surface circulation patterns, *J. Geophys. Res.*, *109*, C05015, doi:10.1029/2003JC002241.